



Title	Studies on interparticle charge-transfer excitation : Novel band-structure analysis of semiconducting metal-oxide photocatalysts based on energy-resolved distribution of electron traps
Author(s)	沈, 陽
Citation	北海道大学. 博士(環境科学) 甲第14345号
Issue Date	2021-03-25
DOI	10.14943/doctoral.k14345
Doc URL	http://hdl.handle.net/2115/88968
Type	theses (doctoral)
File Information	Shen_Yang.pdf



[Instructions for use](#)

A doctoral dissertation

Studies on interparticle charge-transfer excitation: Novel band-
structure analysis of semiconducting metal-oxide photocatalysts
based on energy-resolved distribution of electron traps

(粒子間電荷移動励起に関する研究－電子トラップ密度のエネルギー分布にも
とづく半導体金属酸化物光触媒の新規バンド構造解析)

Yang Shen

Division of Environmental Materials Science
Graduate School of Environmental Science
Hokkaido University

2021

Table of contents

GENERAL INTRODUCTION	1
1.1 <i>Metal-oxide Powders</i>	1
1.1.1 <i>Band Structure of Metal Oxides</i>	1
1.1.2 <i>Hetero-contact Degree of Metal-oxide Mixtures</i>	3
1.2 <i>Energy-resolved Distribution of Electron Traps</i>	4
1.2.1 <i>Electron-trap Density</i>	4
1.2.2 <i>Reversed Double-beam Photoacoustic Spectroscopy</i>	6
1.3 <i>Purpose of This Study</i>	10
1.4 <i>References</i>	10
INTERPARTICLE CHARGE-TRANSFER EXCITATION BETWEEN ADJOINED ANATASE AND RUTILE PARTICLES.....	19
2.1 <i>Introduction.....</i>	19
2.2 <i>Experimental</i>	20
2.2.1 <i>Materials</i>	20
2.2.2 <i>Photoacoustic Spectroscopy (PAS) and Reversed Double-beam Photoacoustic Spectroscopy (RDB-PAS) Measurement</i>	20
2.2.3 <i>Scanning Electron Microscope (SEM) Measurement</i>	22
2.3 <i>Results and Discussion</i>	22
2.3.1 <i>Energy-resolved Distribution of Electron Traps Pattern of Metal-oxide Mixture Prepared by Different Mixing Procedures.....</i>	22
2.3.2 <i>Simulation of Energy-Resolved Distribution of Electron Traps</i>	27
2.3.3 <i>Interparticle Charge-Transfer Excitation</i>	28

2.4	<i>Conclusions</i>	30
2.5	<i>References</i>	31
EVALUATION OF RELATIVE BAND STRUCTURE OF SEMICONDUCTING METAL OXIDES.....		
3.1	<i>Introduction</i>	33
3.2	<i>Experimental</i>	33
3.2.1	<i>Materials</i>	33
3.2.2	<i>Photoacoustic Spectroscopy (PAS) and Reversed Double-beam Photoacoustic Spectroscopy (RDB-PAS) Measurement</i>	34
3.2.3	<i>Photoelectron Yield Spectroscopic (PYS) Measurement</i>	34
3.3	<i>Results and Discussion</i>	34
3.3.1	<i>Maximum Energy Shift (ΔE_{max}) Values of 50/50 Mixtures of Different Kinds of Titania</i>	34
3.3.2	<i>Maximum Energy Shift (ΔE_{max}) Values of Different Anatase Contents in Mixtures</i>	36
3.3.3	<i>Evaluation of the Relative Band Structure of Titania</i>	37
3.3.4	<i>Evaluation of the Band Structure of Anatase and Rutile Isolated from P25</i>	45
3.3.5	<i>Evaluation of the Relative Band Structure for Various Metal-oxides</i>	50
3.4	<i>Conclusions</i>	52
3.5	<i>References</i>	52
QUANTITATIVE MEASUREMENT OF THE HETERO-CONTACT DEGREE OF METAL-OXIDE MIXTURES		
4.1	<i>Introduction</i>	55
4.2	<i>Experimental</i>	55
4.2.1	<i>Materials</i>	55

4.2.2	<i>Photoacoustic Spectroscopy (PAS) and Reversed Double-beam</i>	
	<i>Photoacoustic Spectroscopy (RDB-PAS) Measurement</i>	56
4.2.3	<i>Scanning Electron Microscope (SEM) Measurement</i>	56
4.2.4	<i>X-ray Diffraction (XRD) Measurement</i>	56
4.2.5	<i>Brunner–Emmet–Teller (BET) Measurement</i>	56
4.2.6	<i>Gas Phase Reaction Performance Measurement</i>	56
4.3	<i>Results and Discussion</i>	57
4.3.1	<i>Quantitative Analysis of Hetero-contact Degree of Mixture Samples of</i>	
	<i>Anatase and Rutile</i>	57
4.3.2	<i>Hetero-contact Degree of Mixture Samples of Anatase and Rutile Prepared</i>	
	<i>by Different Mixing Time</i>	62
4.3.3	<i>Hetero-contact Degree of Mixture Samples of Anatase and Rutile Prepared</i>	
	<i>by Different Anatase Contents</i>	65
4.3.4	<i>Gas Phase Photocatalytic Reaction Performance of Mixtures with</i>	
	<i>Different Hetero-contact degree</i>	69
4.4	<i>Conclusions.....</i>	71
4.5	<i>References</i>	72
	GENERAL CONCLUSIONS	75
5.1	<i>Conclusions.....</i>	75
5.2	<i>Future Aspects.....</i>	76
5.3	<i>Original Papers Covering This Thesis</i>	77
	ACKNOWLEDGEMENT.....	79

1.1 Metal-oxide Powders

1.1.1 Band Structure of Metal Oxides

Metal oxide samples, which are widely used in large quantities as chemical functional materials such as photocatalysts, catalysts, sensors, and oxygen-carriers are categorized as semiconductors or insulators based on its electronic energy structure and the band structure composed of an electron-filled valence band (VB), electron-vacant conduction band (CB) and forbidden band (band gap) separating them from each other [Ohtani 2014], though it seems the real band structure of the metal oxides is still speculative and only conduction band bottom (CBB) and valence band top (VBT) positions have been discussed.

Generally, the band gaps of metal-oxide powders which depend on crystalline composition can be estimated by diffuse reflectance spectroscopy (DRS). In the diffuse reflectance spectroscopy measurement, light was introduced through an aperture into a prism because the metal-oxide powders are normally strong scattering substances, and the light irradiation to the flat surface of powder sample applied onto a sample holder to obtain the spectrum. The value of 100 minus reflectance shows absorption, and bandgap energy was estimated by Kubelka-Munk (K-M) function. The two most common crystalline forms of titanium(IV) oxide (titania) which was the most widely used metal oxide for photocatalytic applications [Fujishima 2000/ Hoffmann 1995/ Shiraishi 2008], are anatase and rutile. It is well known that the bandgaps of anatase and rutile are ca. 3.2 eV [Tang 1993] and 3.0 eV [Minoura 1985], respectively.

Scaife et al. [Scaife 1980] reported that since the valence band consists of O 2p orbital is almost constant at 2.94 V vs SHE based on relations between bandgap and flat band potential, the energy level of valence-band top (VBT) of metal oxides has no connection with the kinds of metals. Therefore, based on the bandgaps of anatase and rutile, as shown in Fig. 1-1a, the conduction band bottom (CBB) of anatase was believed to be ca. 0.2 eV higher than that of rutile due to its larger bandgap.

Since this is just simple estimation and there were exceptions of the relations, other researchers have also done in-depth research on valence-band top (VBT). Kavan et al.

[Kavan 1996] determined the flat-band potential of anatase and rutile were -0.16 and +0.04 eV vs SHE at pH = 0 by electrochemical impedance analysis indicating that the conduction band of anatase is 0.2 eV above that of rutile, this is consistent with estimation of band structure of anatase and rutile shown in Fig. 1-1a. However, Xiong et al. [Xiong 2007] have reported that they determined the work function of anatase is 0.2 eV higher than that of rutile suggesting that the conduction band of anatase is 0.2 eV below that of rutile, as shown in Fig. 1-1b. Scanlon et al. [Scanlon 2013] claimed that the valence band of anatase was found to be at 0.39 ± 0.02 eV higher binding energy than that of rutile through a combination of materials simulation techniques and X-ray photoemission experiments, and this result supports the band structure of Fig. 1-1b.

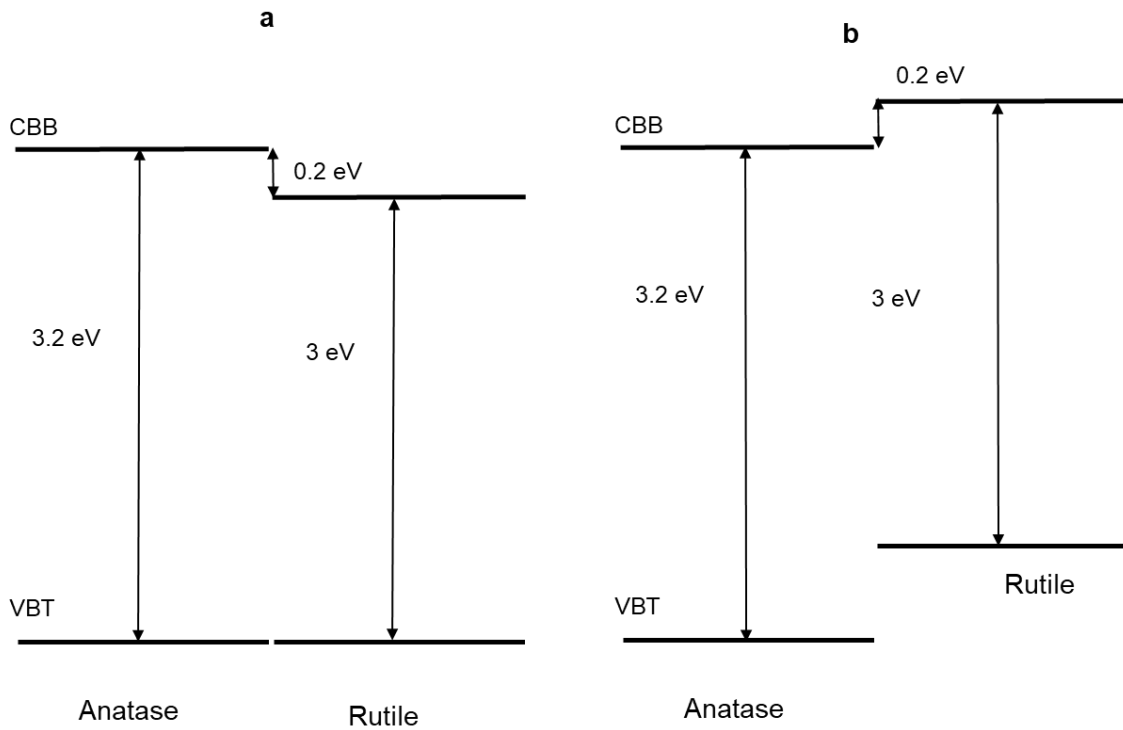


Fig. 1-1 a, Band structure of anatase and rutile based on the result Scaife reported [Scaife 1980]. b, Band structure of anatase and rutile based on the result Xiong and Scanlon reported [Xiong 2007/ Scanlon 2013].

Different from experimental measurements, same researchers [Zhang 2014/ Landmann 2012/ Yan 2013/] have also conducted research of band structure based on materials simulation techniques, the result of Scanlon [Scanlon 2013] includes the materials simulation result. Zhang et al. [Zhang 2014] studied the band structure of three crystal phases titania (anatase, rutile and brookite) through the first-principle density functional theory calculation.

In general, although the band structure have been studied a lot through various experimental measurements and materials simulation techniques [Wang 2011/ Kavan 1996/ Xiong 2007/ Tang 1993/ Minoura 1985/ Scanlon 2013/ Zhang 2014/ Tsuji 2014/ Fujisawa 2017/ Li 2012/ Pfeifer 2013/ Mi 2015], the real band structure of the metal oxides is still speculative and only conduction band bottom (CBB) and valence band top (VBT) positions have been discussed. The previous research suggest in reversed double-beam photoacoustic spectroscopy (RDB-PAS) measurement electrons may excited to ETs from higher DOS (density of states) part of the valence band (h-DOS(VB)) which have lower energy than VBT [Nitta 2018]. The practical h-DOS, which enable to cause photoabsorption, of materials is need to pay more attention.

1.1.2 Hetero-contact Degree of Metal-oxide Mixtures

Semiconducting metal-oxides such as titania have been widely used in a variety of applications in the environmental and energy fields [Fujishima 2000/ Fujishima 2008/Hoffmann 1995/Shiraishi 2008/Hashimoto 2005]. The design and development of heterostructured photocatalysts is a promising strategy to improve photocatalytic performance. Many researchers have suggested that the reason for the activity in photocatalytic performance of heterostructured photocatalyst is that the electron-hole recombination is reduced by the charge transfer between the original particles of the heterostructured photocatalyst sample [Bickley 1991/Kamat 1993/ Hurum 2003/ Ohno 2003/ Sun 2018/ Nakajima 2005/ Rawool 2018/ Yang 2013/ Ohno 2001/ Wang 2012/ Ng 2010/ Manga 2009]. Irie et al. argued that Cu(II)-grafted titania samples are sensitive to visible light through visible light initiates interfacial charge transfer (IFCT) [Creutz 2005/Irie 2008/Irie 2009/Yu 2010]. It is easy to expect that when such electron transfer occurs, there must be an electronic interaction between various particles, and direct observation of the interaction could provide significant information for both practical and fundamental studies of functional metal-oxide materials, e.g., photocatalyst. However, there is no experimental evidence of electronically interacted particles. An experimental evidence of electronic interaction is very important. In addition, since the electronic interaction require adequate contact of various particles, design and development of method to evaluation the hetero-contact condition which means the state of contact between different kinds of particles is also very important.

Siiriä et al. [Siiriä 2009] claimed that they developed a new mathematical simulation technique to determine the hetero-contact degree for a given system. However, this method requires the information of the locations of the particles both in the original

state and the state for which the degree of hetero-contact is calculated. Therefore, this method is only suitable for simulation purpose. Cleary et al. [Cleary 1998] have reported that they developed a method can obtain the segregation and mixing in granular flows which have a complex particle distribution through taking local averages of the desired property (mass, density or colour) which represent the extent of mixing. However, this method can only be used to estimate the degree of hetero-contact of macroscopic large particles, and give no information about the hetero-contact of nanoparticles. Kim et al. [Kim 2007] tried to find a suitable quantitative characterization method for the hetero-contact degree for nanocomposites, they tried to use TEM to measure the hetero-contact degree. However, the quantitative hetero-contact degree of these methods is obtained by mathematically processing the results of small-scale TEM images, not directly macroscopic measured experimentally.

In general, the hetero-contact degree of nanoparticles was either defined by mathematical simulation [Siiriä 2009/ Yeoh 2005/ Kim 2007] or estimated based on calculating the probability distribution of local averages of the desired property [Cleary 1998/ Suetsugu 1990/ Bur 2004]. Therefore, technique which can quantitatively evaluate the hetero-contact condition between nanoparticles should be developed.

1.2 Energy-resolved Distribution of Electron Traps

1.2.1 Electron-trap Density

Most metal oxides are categorized as n-type semiconductors which have electron-filled donor levels below CBB due to the oxygen anions of metal oxides samples are easily apt to be detached to leave electrons in an oxygen defect [Ohtani 2013]. These electron-filled donor levels will lose electrons and become electron traps (ETs) when donor electrons flow out to adsorbed water or surface hydroxyl groups. It is well known that metal oxides, such as titanium(IV) oxide, turn blue when reduced by photoirradiation in the presence of electron donors in deaerated conditions or calcination under hydrogen atmosphere or in vacuum. The blue color of titania is attributed to that some tetravalent titanium (Ti^{4+}) ions are reduced by electrons excited in the conduction band (CB) to form trivalent titanium (Ti^{3+}) ions [Howe 1985/ Kawaguchi 1968/ Ghosh 1969/ Inoue 1970/ Kölle 1985/ Hasegawa 1971]. In other words, metal-oxide powders have electron traps (ETs) on the surface.

The molar amount of electron traps which predominantly located on the surface of metal oxides have been analyzed by various methods. Shiraishi et al. [Shiraishi 2013/

Shiraishi 2014] estimated the electron-trap density on the surface of titania powder through diffuse-reflectance infrared Fourier transform (DRIFT) analysis of nitrobenzene adsorbed onto titania powder. Ikeda et al. [Ikeda 2003] reported the measurement of total density of electron traps in titania samples by photochemical method. As shown in Fig. 1-2, in the photochemical method measurement, titania suspensions were under UV irradiation in the presence of electron donors such as triethanolamine and methanol to fill all electron traps with electrons, then add methyl viologen cation (MV^{2+}). The MV^{2+} will be reduced into methyl viologen cation radical ($MV^{\bullet+}$) by the electrons trapped by electron traps. The total density (total molar amount) of electron traps can be estimated by measuring the molar amount of $MV^{\bullet+}$ through photoabsorption spectroscopy.

The deep-level transient spectroscopy (DLTS) is considered to be used to measure the energy-resolved distribution of electron traps (ERDT) of metal-oxide powders by several researchers [Lang 1974/Miyagi 2001/Miyagi 2004]. However, Nitta et al. considered that DLTS detects only deep traps in the bulk of metal-oxide samples [Nitta 2018]. As shown in Fig. 1-2, Ikeda et al. [Ikeda 2003] reported successful ERDT analysis by photochemical method of anatase and rutile through added MV^{2+} by changing the pH of photoirradiated titania suspensions from lower side to higher side. However, this photochemical method requires very careful operation and it takes a long time to obtain the energy-resolved distribution of electron traps (ERDT) of metal-oxide powders. Buchalska et al. [Buchalska 2015] reported a spectroelectrochemical method to measure the energy-resolved distribution of electron traps (ERDT), but the electrode preparation

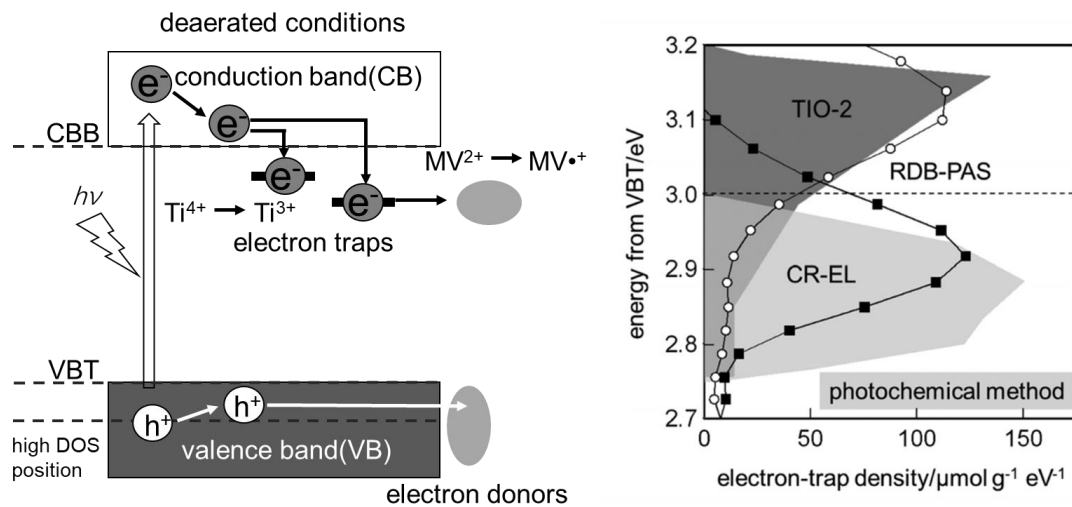


Fig. 1-2 Analysis of energy-resolved distribution of electron traps (ERDT) [Ikeda 2003/ Nitta 2016].

process in this method might change the surface structure of samples to cause the change of ERDT.

1.2.2 Reversed Double-beam Photoacoustic Spectroscopy

The phenomenon of photoacoustic (PA) effect which generation of sound by a light-absorbing sample irradiated by the intermittent light that is the principle of photoacoustic spectroscopy (PAS), was discovered by Bell, the inventor of the telephone, in 1880 [Bell 1880]. Photoacoustic spectroscopy (PAS) was only used to characterize gaseous samples as a gas spectroscopy until Rosencwaig et al. [Rosencwaig 1976] established a theory of solid PA effects in 1976, and PAS has been widely used for solid samples since then. As shown in Fig. 1-3, when a light-absorbing sample (gas, liquid or solid) irradiated by the intermittent light, electronic, rotational or vibrational excitation occurs and heat will be released through a part of those excited states is deactivated. This heat expands the volume of the irradiated sample, and then the expanded sample will be shrunk at the interval of intermittent photoabsorption, sound with a frequency that is same with the intermittent light will be created through this expansion-shrinking cycles caused by intermittent light irradiation [Nitta 2018]. Therefore, the photoacoustic spectroscopy (PAS) can obtain the photoabsorption spectroscopy by detect the sound wave caused by intermittent light.

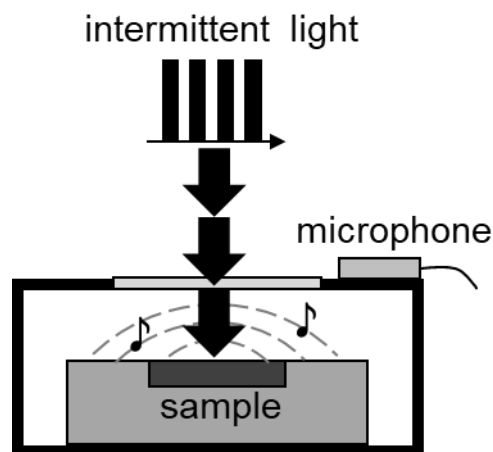


Fig. 1-3 Schematic image of photoacoustic spectroscopy.

For photoacoustic spectroscopy (PAS), since there is no need to detect the light intensity after irradiating the sample like transmission/reflection spectroscopy, the

influence of light scattering can be avoided. In addition, since the PA signal is proportional to the intensity of the excitation light and the PA signal measurement can use a microphone that does not depend on the wavelength of the irradiated light, it is possible to perform highly sensitive measurement by optimizing the light source and sensor (microphone). In view of above advantages of PAS, as one of the best techniques for measuring the light absorption of powder samples, PAS is applied to the characterization of metal oxide powders such as zinc oxide (ZnO), bismuth oxide (Bi₂O₃) [Toyoda 1998], and titania powders [Toyoda 2000].

Since the successful application of PAS to metal oxide powders, double-beam photoacoustic spectroscopy (DB-PAS) was developed for the characterization of semiconducting metal oxide powders such as titania [Murakami 2006/Murakami 2007/Murakami 2007b/Murakami 2008]. In the double-beam photoacoustic spectroscopy (DB-PAS) measurement, two kinds of light source are used, continuous light and intermittent light. The electrons in the valence band of sample are excited to the electron traps via the conduction band by continuous light and accumulated in electron traps since holes are scavenged by methanol vapor as electron donor, and these accumulated electrons can absorb visible light caused the increase in light absorption. At the same time, the intermittent light can detect the photoabsorption for accumulated electrons by PAS and the increase in photoabsorption measured by the PA signal corresponds to the density of electron traps [Murakami 2007]. Therefore, the total density of electron traps can be estimated by double-beam photoacoustic spectroscopy (DB-PAS).

Since the successful application of DB-PAS to estimate the total density of electron traps of semiconducting metal oxide powders, reversed double-beam photoacoustic spectroscopy (RDB-PAS) has been developed by modifying DB-PAS to measure the energy-resolved distribution of electron traps (ERDT) of metal-oxide powders [Nitta 2016/ Nitta 2018/ Nitta 2019]. In PAS and DB-PAS, a PA spectrum of sample was obtained by a wavelength-scanned modulated (chopped) intermittent light beam creating a PA signal, for DB-PAS there is another continuous light (fixed wavelength), which does not have any effect on the PA signal, is overlapped with the wavelength-scanned intermittent light. In reversed double-beam photoacoustic spectroscopy (RDB-PAS), contrary to the wavelength scan mode in DB-PAS, continuous light is wavelength-scanned and intermittent light generating the PA signal is wavelength-fixed.

As shown in Fig. 1-4, in reversed double-beam photoacoustic spectroscopy (RDB-PAS) measurement, electrons in the valence band (VB) of sample are directly excited to the electron traps (ETs) by continuous light and accumulated in electron traps since holes are scavenged by methanol vapor as electron donor. Since the continuous light (excitation

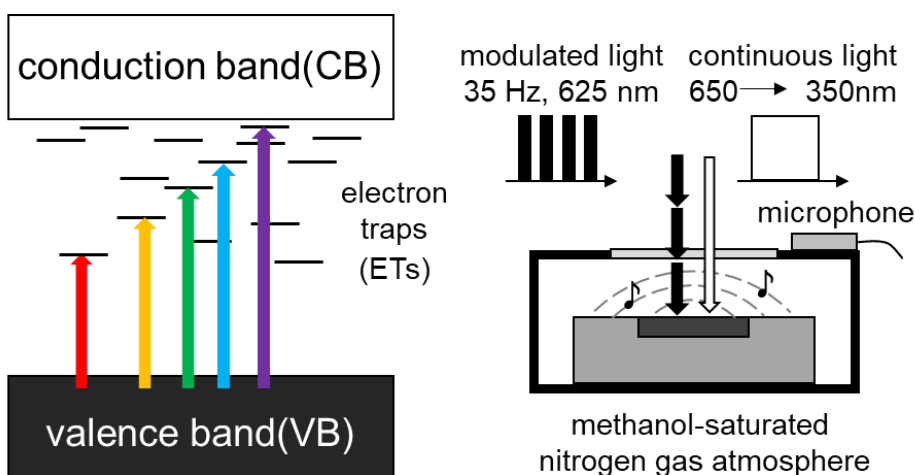


Fig. 1-4 Schematic image of reversed double-beam photoacoustic spectroscopy.

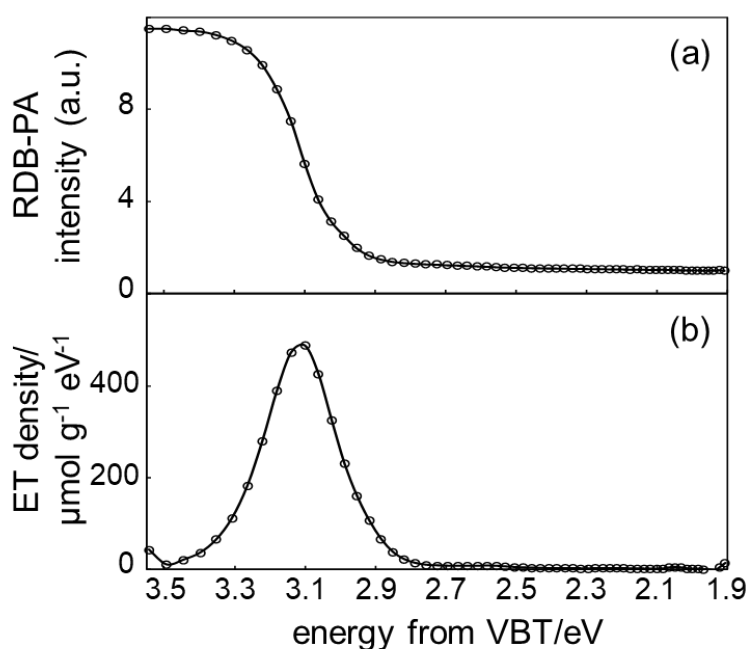


Fig. 1-5 (a) raw RDB-PA spectrum and (b) differentiated spectrum of (a) for anatase sample (ST-21)

light) in RDB-PAS is wavelength-scanned from longer wavelength to shorter wavelength, the electrons accumulated in the electron traps (ETs) from lower energy side to higher energy side. These accumulated electrons can absorb light caused the increase in photoabsorption. Simultaneously, modulated monochromatic light is irradiated to the sample to detect the increase of photoabsorption by photoacoustic (PA) signal which corresponds to the electron-filled ETs (detail of the setups and procedures see 2.2.2). The PA signal was detected by a microphone and plotted against energy of continuous excitation light to obtain RDB-PAS spectrum (Fig. 1-5(a)). The obtained RDB-PAS

spectrum which is a plot of total accumulated electron-trap density as a function of photon energy of continuous light was differentiated from the lower energy side to higher energy side to obtain ERDT. Then, the obtained signal value was converted into electron trap density in unit of $\text{g}^{-1} \text{eV}^{-1}$ by the conversion factor determined with the reported total electron trap density measured by photochemical method [Ikeda 2003] to obtain an ERDT pattern as a function of energy as reference to the VBT (valence-band top) ((Fig. 1-5(b)). To obtain bar-graph type ERDT pattern as shown in Fig. 1-6, the above-mentioned ERDT was replotted with a 0.05-eV pitch. The ERDT/CBB patterns of ST-21(anatase) and ST-G1(rutile) are shown in Fig. 1-6, it shows the density of electron traps along the energy distribution.

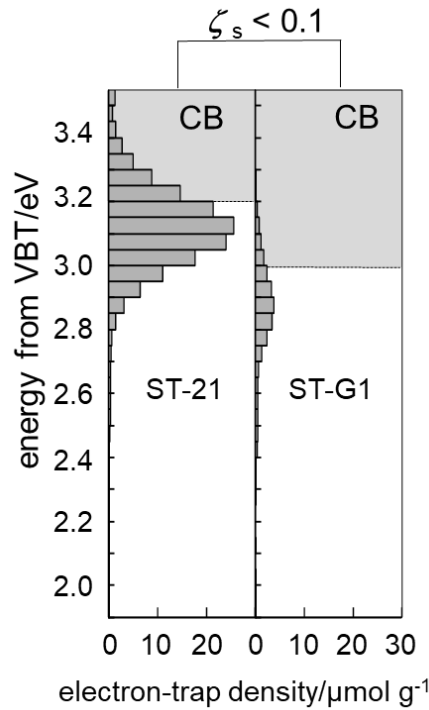


Fig. 1-6 ERDT/CBB pattern of ST-21(anatase) and ST-G1(rutile).

To compare two and more ERDT/CBB patterns, degrees of coincidence, ζ , were introduced [Nitta 2016/ Nitta 2018/ Nitta 2019], which is composed of three parameters; ζ_s for coincidence of the ERDT pattern shape (peak position and shape), ζ_D for similarity of the total density of electron traps, ζ_C for similarity of the CBB position to give $\zeta = \zeta_s \times \zeta_D^{1/2} \times \zeta_C^2$. In this study, only ζ_s was used as a comparison and calculated as

$$\zeta_s = 1 - \frac{\int |f(1) - \alpha f(2)|}{\int f(1)},$$

where integrated electron trap distribution (f as a function of energy from VBT) in the measured energy range is equal to total density of electron traps, D , $f(1)$ and $f(2)$ are defined by comparing their total ET density; $D(1) < D(2)$, and α is determined by the

least squares method so as to minimize integrated $(f(1) - \alpha f(2))^2$ in the measured energy range. The ζ_s value of 1 means 100% coincidence in the pattern shape (without considering the absolute density of electron traps). For ST-21(anatase) and ST-G1(rutile) shown in Fig. 1-6, $\zeta_s < 0.1$ means the ERDT pattern shape of ST-21(anatase) and ST-G1(rutile) are totally different. Thus, the reversed double-beam photoacoustic spectroscopy (RDB-PAS) is a powerful tool to measure ERDT for identification and characterization of metal-oxide powders.

1.3 Purpose of This Study

The band structure of semiconducting metal-oxides, which impact the physical and chemical properties of metal oxides, is very important, though it seems the real band structure of metal oxides is still speculative and only conduction-band bottom (CBB) and valence-band top (VBT) positions have been discussed mainly. The hetero-contact degree of nanoparticles which is important for design and development of heterostructured photocatalysts is a new concept and has not been measured so far. Since a novel method for identification and characterization of metal-oxide powders with energy-resolved distribution of electron traps (ERDT) measured by reversed double-beam photoacoustic spectroscopy (RDB-PAS) have been developed. In this study, ERDT analysis using RDB-PAS is expected to be applicable to estimation of band structure of metal-oxide samples and provides quantitative measurement of the hetero-contact degree.

1.4 References

[Ohtani 2014] Ohtani B. Revisiting the fundamental physical chemistry in heterogeneous photocatalysis: its thermodynamics and kinetics[J]. *Physical chemistry chemical physics*, **2014**, 16(5): 1788-1797.

Fujishima 2000 Fujishima A, Rao T N, Tryk D A. Titanium dioxide photocatalysis[J]. *Journal of photochemistry and photobiology C: Photochemistry reviews*, **2000**, 1(1): 1-21.

Hoffmann 1995 Hoffmann M R, Martin S T, Choi W, et al. Environmental applications of semiconductor photocatalysis[J]. *Chemical reviews*, **1995**, 95(1): 69-96.

Shiraishi 2008 Shiraishi Y, Hirai T. Selective organic transformations on titanium oxide-based photocatalysts[J]. *Journal of Photochemistry and Photobiology C: Photochemistry Reviews*, **2008**, 9(4): 157-170.

Tang 1993 Tang H, Berger H, Schmid P E, et al. Photoluminescence in TiO₂ anatase single crystals[J]. *Solid State Communications*, **1993**, 87(9): 847-850.

Minoura 1985 Minoura H, Nasu M, Takahashi Y. Comparative studies of photoelectrochemical behaviours of rutile and anatase electrodes prepared by OMCVD technique[J]. *Berichte der Bunsengesellschaft für physikalische Chemie*, **1985**, 89(10): 1064-1069.

Scaife 1980 Scaife D E. Oxide semiconductors in photoelectrochemical conversion of solar energy[J]. *Solar Energy*, **1980**, 25(1): 41-54.

Kavan 1996 Kavan L, Grätzel M, Gilbert S E, et al. Electrochemical and photoelectrochemical investigation of single-crystal anatase[J]. *Journal of the American Chemical Society*, **1996**, 118(28): 6716-6723.

Xiong 2007 Xiong G, Shao R, Droubay T C, et al. Photoemission electron microscopy of TiO₂ anatase films embedded with rutile nanocrystals[J]. *Advanced Functional Materials*, **2007**, 17(13): 2133-2138.

Scanlon 2013 Scanlon D O, Dunnill C W, Buckeridge J, et al. Band alignment of rutile and anatase TiO₂ [J]. *Nature materials*, **2013**, 12(9): 798-801.

Zhang 2014 Zhang J, Zhou P, Liu J, et al. New understanding of the difference of photocatalytic activity among anatase, rutile and brookite TiO₂[J]. *Physical Chemistry Chemical Physics*, **2014**, 16(38): 20382-20386.

Nitta 2016 Nitta A, Takase M, Takashima M, et al. A fingerprint of metal-oxide powders: energy-resolved distribution of electron traps[J]. *Chemical Communications*, **2016**, 52(81): 12096-12099.

Nitta 2019 Nitta A, Takashima M, Takase M, et al. Identification and characterization of titania photocatalyst powders using their energy-resolved distribution of electron traps as a fingerprint[J]. *Catalysis Today*, **2019**, 321: 2-8.

Nitta 2018 Nitta A, Takashima M, Murakami N, et al. Reversed double-beam photoacoustic spectroscopy of metal-oxide powders for estimation of their energy-resolved distribution of electron traps and electronic-band structure[J]. *Electrochimica acta*, **2018**, 264: 83-90.

Buchalska 2015 Buchalska M, Kobielusz M, Matuszek A, et al. On oxygen activation at rutile-and anatase-TiO₂[J]. *ACS Catalysis*, **2015**, 5(12): 7424-7431.

Fujishima 2008 Fujishima A, Zhang X, Tryk D A. TiO₂ photocatalysis and related surface phenomena[J]. *Surface science reports*, **2008**, 63(12): 515-582.

Hashimoto 2005 Hashimoto K, Irie H, Fujishima A. TiO₂ photocatalysis: a historical overview and future prospects[J]. *Japanese journal of applied physics*, **2005**, 44(12R): 8269.

Creutz 2005 Creutz C, Brunschwig B S, Sutin N. Interfacial charge-transfer absorption: semiclassical treatment[J]. *The Journal of Physical Chemistry B*, **2005**, 109(20): 10251-10260.

Irie 2008 Irie H, Miura S, Kamiya K, et al. Efficient visible light-sensitive photocatalysts: grafting Cu (II) ions onto TiO₂ and WO₃ photocatalysts[J]. *Chemical Physics Letters*, **2008**, 457(1-3): 202-205.

Irie 2009 Irie H, Kamiya K, Shibamura T, et al. Visible light-sensitive Cu (II)-grafted TiO₂ photocatalysts: activities and X-ray absorption fine structure analyses[J]. *The Journal of Physical Chemistry C*, **2009**, 113(24): 10761-10766.

Yu 2010 Yu H, Irie H, Hashimoto K. Conduction band energy level control of titanium dioxide: toward an efficient visible-light-sensitive photocatalyst[J]. *Journal of the American Chemical Society*, **2010**, 132(20): 6898-6899.

Bickley 1991 Bickley R I, Gonzalez-Carreno T, Lees J S, et al. A structural investigation of titanium dioxide photocatalysts[J]. *Journal of Solid state chemistry*, **1991**, 92(1): 178-190.

Kamat 1993 Kamat P V. Photochemistry on nonreactive and reactive (semiconductor) surfaces[J]. *Chemical Reviews*, **1993**, 93(1): 267-300.

Hurum 2003 Hurum D C, Agrios A G, Gray K A, et al. Explaining the enhanced photocatalytic activity of Degussa P25 mixed-phase TiO₂ using EPR[J]. *The Journal of Physical Chemistry B*, **2003**, 107(19): 4545-4549.

Ohno 2003 Ohno T, Tokieda K, Higashida S, et al. Synergism between rutile and anatase TiO₂ particles in photocatalytic oxidation of naphthalene[J]. *Applied Catalysis A: General*, **2003**, 244(2): 383-391.

Sun 2018 Sun X, Chang Y, Cheng Y, et al. Band alignment-driven oxidative injury to the skin by anatase/rutile mixed-phase titanium dioxide nanoparticles under sunlight exposure[J]. *Toxicological Sciences*, **2018**, 164(1): 300-312.

Wang 2011 Wang J, Liu X L, Yang A L, et al. Measurement of wurtzite ZnO/rutile TiO₂ heterojunction band offsets by x-ray photoelectron spectroscopy[J]. *Applied Physics A*, **2011**, 103(4): 1099-1103.

Tsuji 2014 Tsuji E, Fukui K, Imanishi A. Influence of surface roughening of rutile single-crystalline TiO₂ on photocatalytic activity for oxygen photoevolution from water in acidic and alkaline solutions[J]. *The Journal of Physical Chemistry C*, **2014**, 118(10): 5406-5413.

Nakajima 2005 Nakajima H, Mori T, Shen Q, et al. Photoluminescence study of mixtures of anatase and rutile TiO₂ nanoparticles: influence of charge transfer between the nanoparticles on their photoluminescence excitation bands[J]. *Chemical Physics Letters*, **2005**, 409(1-3): 81-84.

Rawool 2018 Rawool S A, Pai M R, Banerjee A M, et al. pn Heterojunctions in NiO: TiO₂ composites with type-II band alignment assisting sunlight driven photocatalytic H₂ generation[J]. *Applied Catalysis B: Environmental*, **2018**, 221: 443-458.

Fujisawa 2017 Fujisawa J, Eda T, Hanaya M. Comparative study of conduction-band and valence-band edges of TiO₂, SrTiO₃, and BaTiO₃ by ionization potential measurements[J]. *Chemical Physics Letters*, **2017**, 685: 23-26.

Li 2012 Li G, Bai Y, Zhang W F. Difference in valence band top of BiVO₄ with different crystal structure[J]. *Materials Chemistry and Physics*, **2012**, 136(2-3): 930-934.

Yang 2013 Yang J S, Liao W P, Wu J J. Morphology and interfacial energetics controls for hierarchical anatase/rutile TiO₂ nanostructured array for efficient photoelectrochemical water splitting[J]. *ACS applied materials & interfaces*, **2013**, 5(15): 7425-7431.

Ohno 2001 Ohno T, Sarukawa K, Tokieda K, et al. Morphology of a TiO₂ photocatalyst (Degussa, P-25) consisting of anatase and rutile crystalline phases[J]. *Journal of Catalysis*, **2001**, 203(1): 82-86.

Wang 2012 Wang X, Xu Q, Li M, et al. Photocatalytic overall water splitting promoted by an α - β phase junction on Ga₂O₃[J]. *Angewandte Chemie*, **2012**, 124(52): 13266-13269.

Ng 2010 Ng J, Xu S, Zhang X, et al. Hybridized nanowires and cubes: a novel architecture of a heterojunctioned TiO₂/SrTiO₃ thin film for efficient water splitting[J]. *Advanced Functional Materials*, **2010**, 20(24): 4287-4294.

Pfeifer 2013 Pfeifer V, Erhart P, Li S, et al. Energy band alignment between anatase and rutile TiO₂[J]. *The Journal of physical chemistry letters*, **2013**, 4(23): 4182-4187.

Mi 2015 Mi Y, Weng Y. Band alignment and controllable electron migration between rutile and anatase TiO₂[J]. *Scientific reports*, **2015**, 5(1): 1-10.

Manga 2009 Manga K K, Zhou Y, Yan Y, et al. Multilayer hybrid films consisting of alternating graphene and titania nanosheets with ultrafast electron transfer and photoconversion properties[J]. *Advanced Functional Materials*, **2009**, 19(22): 3638-3643.

- Siiriä 2009** Siiriä S, Yliruusi J. Determining a value for mixing: Mixing degree[J]. *Powder Technology*, **2009**, 196(3): 309-317.
- Kim 2007** Kim D, Lee J S, Barry C M F, et al. Microscopic measurement of the degree of mixing for nanoparticles in polymer nanocomposites by TEM images[J]. *Microscopy research and technique*, **2007**, 70(6): 539-546.
- Cleary 1998** Cleary P W, Metcalfe G, Liffman K. How well do discrete element granular flow models capture the essentials of mixing processes?[J]. *Applied Mathematical Modelling*, **1998**, 22(12): 995-1008.
- Suetsugu 1990** Suetsugu Y, Kikutani T, Kyu T, et al. An experimental technique for characterizing dispersion in compounds of particulates in thermoplastics using small-angle light scattering[J]. *Colloid and Polymer Science*, **1990**, 268(2): 118-131.
- Bur 2004** Bur A J, Roth S C, Lee Y H, et al. A dielectric slit die for in-line monitoring of polymer compounding[J]. *Review of scientific instruments*, **2004**, 75(4): 1103-1109.
- Landmann 2012** Landmann M, Rauls E, Schmidt W G. The electronic structure and optical response of rutile, anatase and brookite TiO₂[J]. *Journal of physics: condensed matter*, **2012**, 24(19): 195503.
- Yan 2013** Yan H, Wang X, Yao M, et al. Band structure design of semiconductors for enhanced photocatalytic activity: the case of TiO₂[J]. *Progress in Natural Science: Materials International*, **2013**, 23(4): 402-407.
- Yeoh 2005** Yeoh S L, Papadakis G, Yianneskis M. Determination of mixing time and degree of homogeneity in stirred vessels with large eddy simulation[J]. *Chemical Engineering Science*, **2005**, 60(8-9): 2293-2302.
- Ohtani 2013** Ohtani B. Titania photocatalysis beyond recombination: a critical review[J]. *Catalysts*, **2013**, 3(4): 942-953.
- Hasegawa 1971** Hasegawa S, Kawaguchi T. Surface properties and photoconductivity of hydrogenreduced titanium (IV) oxide[J]. *Nihon Kagaku Zasshi*, **1971**, 92: 389-392.

Howe 1985 Howe R F, Gratzel M. EPR observation of trapped electrons in colloidal titanium dioxide[J]. *The Journal of Physical Chemistry*, **1985**, 89(21): 4495-4499.

Inoue 1970 Inoue Y, Hasegawa S, Kawaguchi T. Surface properties and catalytic function of a few metal oxides[J]. *Nippon Kagaku Zasshi*, **1970**, 91: 1034-1038.

Kawaguchi 1968 Kawaguchi S, Hasegawa S, Kaseda K, et al. Studies on the surface electron traps in photoconductors (I) DPPH method and hammett method[J]. *Denshi Shashin*, **1968**, 8: 92-100.

Kawase 2010 Kawase S, Sugimoto K, Fujiwara R, et al. Quantitative Analysis of Amorphous Contents in Photocatalytic Titania Powders[J]. *Bunseki Kagaku/Japan Analyst*, **2010**, 59(10).

Kölle 1985 Koelle U, Moser J, Graetzel M. Dynamics of interfacial charge-transfer reactions in semiconductor dispersions. Reduction of cobaltoceniumdicarboxylate in colloidal titania[J]. *Inorganic chemistry*, **1985**, 24(14): 2253-2258.

Ghosh 1969 Ghosh A K, Wakim F G, Addiss Jr R R. Photoelectronic processes in rutile[J]. *Physical Review*, **1969**, 184(3): 979.

Shiraishi 2013 Shiraishi Y, Hirakawa H, Togawa Y, et al. rutile crystallites isolated from Degussa (Evonik) P25 TiO₂: Highly efficient photocatalyst for chemoselective hydrogenation of nitroaromatics[J]. *Acs Catalysis*, **2013**, 3(10): 2318-2326.

Shiraishi 2014 Shiraishi Y, Hirakawa H, Togawa Y, et al. Noble-metal-free deoxygenation of epoxides: titanium dioxide as a photocatalytically regenerable electron-transfer catalyst[J]. *ACS Catalysis*, **2014**, 4(6): 1642-1649.

Lang 1974 Lang D V. Deep-level transient spectroscopy: A new method to characterize traps in semiconductors[J]. *Journal of applied physics*, **1974**, 45(7): 3023-3032.

Miyagi 2001 Miyagi T, Ogawa T, Kamei M, et al. Deep level transient spectroscopy analysis of an anatase epitaxial film grown by metal organic chemical vapor deposition[J]. *Japanese Journal of Applied Physics*, **2001**, 40(4B): L404.

Miyagi 2004 Miyagi T, Kamei M, Sakaguchi I, et al. Photocatalytic property and deep levels of Nb-doped anatase TiO₂ film grown by metalorganic chemical vapor deposition[J]. *Japanese journal of applied physics*, **2004**, 43(2R): 775.

Bell 1880 Bell A G. ART. XXXIV.--On the Production and Reproduction of Sound by Light[J]. *American Journal of Science* (1880-1910), **1880**, 20(118): 305.

Rosencwaig 1976 Rosencwaig A, Gersho A. Theory of the photoacoustic effect with solids[J]. *Journal of Applied Physics*, **1976**, 47(1): 64-69.

Toyoda 1998 Toyoda T, Shimamoto S. Effects of Bi₂O₃ impurities in ceramic ZnO on photoacoustic spectra and current-voltage characteristics[J]. *Japanese journal of applied physics*, **1998**, 37(5S): 2827.

Toyoda 2000 Toyoda T, Kawano H, Shen Q, et al. Characterization of electronic states of TiO₂ powders by photoacoustic spectroscopy[J]. *Japanese Journal of Applied Physics*, **2000**, 39(5S): 3160.

Murakami 2006 Murakami N, Mahaney O O P, Torimoto T, et al. Photoacoustic spectroscopic analysis of photoinduced change in absorption of titanium (IV) oxide photocatalyst powders: A novel feasible technique for measurement of defect density[J]. *Chemical physics letters*, **2006**, 426(1-3): 204-208.

Murakami 2007 Murakami, N.; Prieto-Mahaney, O.-O.; Abe, R.; Torimoto, T.; Ohtani, B.; Double-Beam Photoacoustic Spectroscopic Studies on Transient Absorption of Titanium(IV) Oxide Photocatalyst Powders, *J. Phys. Chem. C*, **111**, 11927–11935 (2007).

Murakami 2007b Murakami N, Prieto Mahaney O O, Abe R, et al. Double-beam photoacoustic spectroscopic studies on transient absorption of titanium (IV) oxide photocatalyst powders[J]. *The Journal of Physical Chemistry C*, **2007**, 111(32): 11927-11935.

Murakami 2008 Murakami N, Abe R, Ohtani B. In situ observation of photocatalytic reaction by photoacoustic spectroscopy: Detection of heat of exothermic photocatalytic reaction[J]. *Chemical Physics Letters*, **2008**, 451(4-6): 316-320.

**Interparticle Charge-Transfer Excitation between Adjoined
Anatase and Rutile Particles****2.1 Introduction**

Semiconductor materials such as titania have been widely used in a variety of applications and products in the energy and environmental fields [Fujishima 2000/ Hoffmann 1995/ Shiraishi 2008]. The design and development of hetero-structured photocatalysts is a promising strategy to improve photocatalytic activity. Although many researchers have suggested that the reason for the improvement in photocatalytic performance of hetero-structured photocatalyst is that the electron-hole recombination is reduced by the charge transfer between different kinds of particles [Bickley 1991/ Kamat 1993/ Hurum 2003/ Ohno 2003/ Sun 2018], there is no direct experimental evidence to prove it. Irie et al. reported that Cu(II)-grafted titania samples are sensitive to visible light to be explained by visible light initiates interfacial charge transfer (IFCT) from the valence band (VB) of the photocatalyst to a co-catalyst deposited on the photocatalyst surface, leading to enhancement of light absorption [Creutz 2005/ Irie 2008/ Irie 2009/ Yu 2010]. When such electron transfer occurs, there must have an electronic interaction. Although there are a lot of researchers published papers claiming electron transfer between neighboring particles (without chemical bond) as a key process controlling the overall performance of various functional materials such as those used for photocatalysts, solar cells and batteries. However, it seems that there is no experimental evidence has been reported to show clearly the spatial and energetic overlap of orbitals (or electronic states) of two particles which is an essential requirement for the interparticle electron transfer. An experimental evidence of electronic interaction is very important for the design and development of hetero-structured photocatalysts and visible-light-sensitive photocatalyst and direct observation of the interaction could provide significant information for both fundamental and practical studies on wide range of functional materials.

It is well known that metal oxides, such as titanium (IV) oxide, have electron traps (ETs) on the surface of particle. As reported previously [Nitta 2016/ Nitta 2019/ Nitta 2018/ Buchalska 2015], a novel method for identification and characterization of metal-oxide powders with energy-resolved distribution of electron traps (ERDT) measured by reversed double-beam photoacoustic spectroscopy (RDB-PAS) have been developed. The ERDT pattern which differs depending on the kind of sample reflect the surface structure, the total electron trap (ET) density which shows an almost linear relation with

specific surface area reflect the particle size, and the CBB position, which is obtained by PAS measurement, reflect the bulk structure of metal-oxide samples. Herein, I obtained direct experimental evidence of electronically interaction, interparticle charge-transfer excitation (ICTE) between thoroughly adjoined anatase and rutile particles, through energy-resolved distribution of electron traps (ERDT) analysis [Shen 2020].

2.2 *Experimental*

2.2.1 *Materials*

Commercial samples and samples from Japan Reference Catalyst (JRC-TIO series) supplied by the Catalysis Society of Japan (CSJ) was used. The preparation of metal-oxide mixtures is as follows. Just put two original samples (ST-21 and ST-G1) half to half on the sample holder (no mixing) marked as "mix-0"; equal amounts of ST-21 and ST-G1 were placed in the agate mortar, mixed them by brayed manually for 10 min marked as "mix-H" (heavily mixed); equal amounts of ST-21 and ST-G1 were placed in the agate mortar, gently mixed them with a Teflon spatula manually for 20 min marked as "mix-L" (lightly mixed).

2.2.2 *Photoacoustic Spectroscopy (PAS) and Reversed Double-beam Photoacoustic Spectroscopy (RDB-PAS) Measurement*

The bandgap to estimate conduction band bottom (CBB) position was measured by photoacoustic spectroscopy (PAS). A sample holder filled with sample was set in a laboratory-made PAS cell equipped with a MEMS (micro-electro-mechanical system; SparkFun MEMS Microphone Breakout, INMP401 (ADMP401)) microphone module and a glass window attached on the upper side of the PAS cell. In the PAS measurements, the PAS cell was closed and a light beam generated from a xenon lamp equipped with a grating monochromator (Bunkoiki M10RP) and modulated at 270 Hz by a light chopper irradiated from the upper side of the PAS cell scanning from 450 nm to 350 nm with a 1 nm step. Photoacoustic (PA) signal was detected by a microphone connected to a digital lock-in amplifier (NF Corporation LI5630) and the PA spectra used to estimate the conduction-band bottom (CBB) was recorded with reference to PA spectrum of graphite (Fig. 2-1(a)).

The energy-resolved distribution of electron trap (ERDT) was measured by Reversed Double-beam Photoacoustic Spectroscopy (RDB-PAS), nitrogen saturated with methanol vapor was flowed through a sample-loaded PAS cell for 30 min (nitrogen flow: 30 mL min⁻¹), then the cell was closed. Move the PAS cell into an acrylic box and pass nitrogen through the acrylic box to make sure the acrylic box was filled with nitrogen. Two light beams irradiated from the upper side of the PAS cell through a UV quartz combiner light guide (Moritex, MWS5-1000S-UV3). One light beam (continuous excitation light) was a monochromatic light produced from a xenon lamp equipped with a grating monochromator (Bunkoikeiki M10RP) and scanning from 650 nm to 350 nm with a 5 nm step. The other beam (detection intermittent light) was a 625-nm LED light beam modulated by a digital function generator (NF Corporation DF1906) at 35Hz. The PA signal was detected by a microphone connected to a digital lock-in amplifier (NF Corporation LI5630) and plotted against energy of continuous excitation light (Fig. 2-1(b)). The obtained signal value was converted into electron trap density in unit of $\mu\text{mol g}^{-1} \text{eV}^{-1}$ by the conversion factor determined with the reported total electron trap density measured by photochemical method [Ikeda 2003] to obtain an ERDT pattern (Fig. 2-1(c)). To obtain bar-graph type ERDT pattern as shown in Fig. 1-6, the above-mentioned ERDT was replotted with a 0.05-eV pitch.

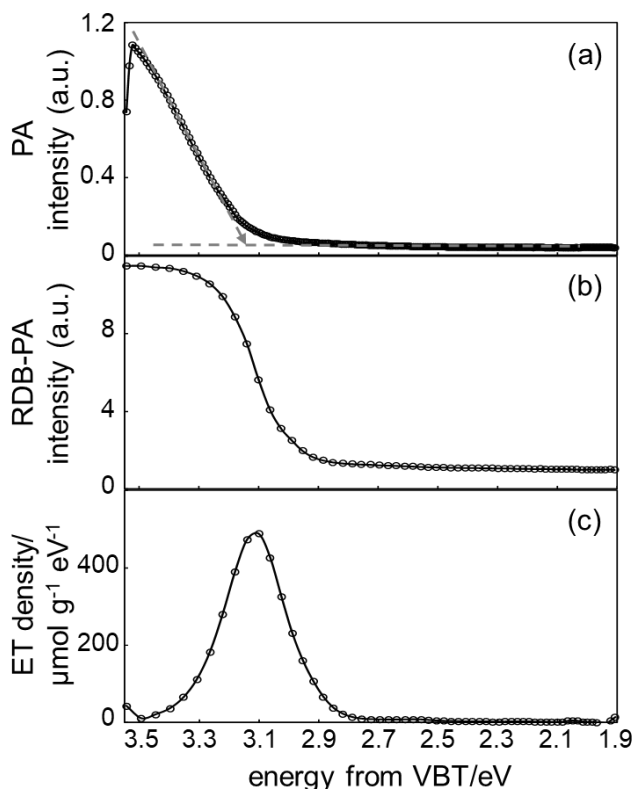


Fig. 2-1 (a) PA spectrum, (b) raw RDB-PA spectrum and (c) differentiated spectrum of (b) for anatase sample (ST-21)

2.2.3 Scanning Electron Microscope (SEM) Measurement

Scanning electron microscopy (SEM) was used to characterize the morphology of the samples by using JEOL JSM-7400F instruments.

2.3 Results and Discussion

2.3.1 Energy-resolved Distribution of Electron Traps Pattern of Metal-oxide Mixture Prepared by Different Mixing Procedures

As reported previously [Nitta 2016/Nitta 2019/Nitta 2018/Buchalska 2015], in RDB-PAS measurement, electrons in the valence band of metal-oxide sample are directly excited to ETs and accumulated in the ETs from the deeper side to the shallower side through wavelength-scanned continuous light, the ERDT pattern shows the density of electron traps along the energy distribution. As shown in Fig. 1-6, electron traps of samples were concentrated around CBB and some of the ETs had energy higher than CBB, however, I generally consider that there is no ETs in conduction band (CB). As shown in Fig. 2-2, one of the possible explanations for this curious trend is overestimation of ET energy which was evaluated as energy from the valence band top (VBT), and the electrons may be excited to ETs from higher DOS (density of states) part of the valence band (h-DOS(VB)) which have lower energy than VBT. It is easy to expect that the photoabsorption coefficient for electrons to be excited to ETs is very small because the process of electrons directly excited to electron traps (ETs) has almost no effect on the ordinary photoabsorption spectrum. Therefore, electrons directly excited to ETs may occur from the h-DOS(VB) not the VBT, and the additional energy (energy difference between VBT and h-DOS(VB)) is required for electrons excited to ETs.

RDB-PAS measurement, which enables detection of ETs predominantly located on the surface of the particle, is one of the most sensitive methods for evaluation of the surface structure. For a mixture sample, it seemed that ERDT patterns of the mixture could be reproduced by simple summation based on the RDB-PAS principle if there was no electronic interaction, however, ERDT patterns of a mixture could not be reproduced by simple summation.

Figure 2-3 shows ERDT/CBB patterns of ST-21(anatase), ST-G1(rutile) and mix-H (a 50/50 mixture of ST-21 and ST-G1). The mixture of ST-21 and ST-G1 was prepared by brayed manually for 10 min, just a physical mixing. It can be seen in Fig. 2-4 that the

Figure 2-4 is ERDT patterns of ST-21 powder before and after braying in an agate mortar as the same procedure of mix-H. Although the total density of ET was a little increased, ζ_s ($0 < \zeta_s < 1$; for calculation, see 1.2.2) which represent the degree of coincidence of ERDT pattern shape was proposed and $\zeta_s = 0.97$ means the ERDT pattern shape of ST-21 powder before and after braying was almost the same. This suggests that mixing (braying) process does not give any influence on the ET distribution, hence the results in Fig. 2-3 that the ERDT patterns of mixture sample was not reproduced by simple summation of two original ERDT patterns cannot be explained by the change of ET distribution by braying.

For further research, mixtures of anatase and rutile samples with different contact conditions (hetero-contact degrees) were prepared by different production methods and their ERDT patterns were evaluated by RDB-PAS. Fig. 2-5 shows the ERDT patterns of ST-21, ST-G1 and their 50/50 mixtures prepared by different production methods (mix-0, L and H for separately loaded, lightly mixed sample and heavily mixed sample. See 2.2.1.), including simulated ERDT patterns with different shift degree (ΔE), named as SIM(ΔE), which were prepared by summing up 50% lower-energy shifted (0 eV and 0.19 eV) ERDT pattern of ST-21 and 50% measured ERDT pattern of ST-G1(no shift), and summation of 65% SIM(0) and 35% SIM(0.19) to reproduce the ERDT pattern of mix-L as discussed later. Interestingly, the ERDT patterns of mix-0, L and H were different depending on the mixture homogeneity, while total ETs of the mixtures were about average of those of ST-21 and ST-G1. The degree of coincidence of the ERDT pattern shape (peak position and shape), ζ_s of mix-0 (ST-21 and ST-G1 were separately loaded on the cell) and simple summation of ERDT patterns of ST-21 and ST-G1 (SIM(0)) showed a relatively higher value (0.80), indicating that the pattern shapes of mix-0 and SIM(0) were very similar (As reported previously that a commercial titania powder samples taken from the same bottle gave ERDT patterns with ζ_s of ca. 0.8 or higher, indicating that samples giving $\zeta_s > 0.8$ can be a relatively higher similarity [Nitta 2016]). Since mix-0 was ST-21 and ST-G1 separately loaded on a measurement cell, it can be assumed that there was almost no electronic interaction between ST-21 and ST-G1 particles. Thus, it can be considered that electron excitation from each VB of original particles to each ETs of original particles occurred independently in mix-0 to give a relatively higher value of ζ_s . On the other hand, ERDT patterns of other mixtures were totally different from that of SIM(0); a peak in energy located around 3.1 eV observed for ST-21 could not be found for mix-L and mix-H, which were mixed with a Teflon spatula for 20 min and brayed for 10 min in an agate mortar, respectively. Obviously, the ERDT patterns of mix-L and mix-H shifted to a lower energy side compared to that of mix-0.

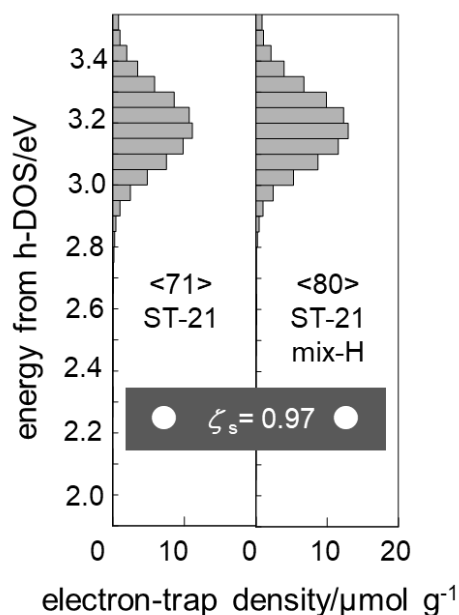


Fig. 2-4 ERDT patterns of an anatase ST-21 powder before and after braying in an agate mortar as the same procedure of mix-H.

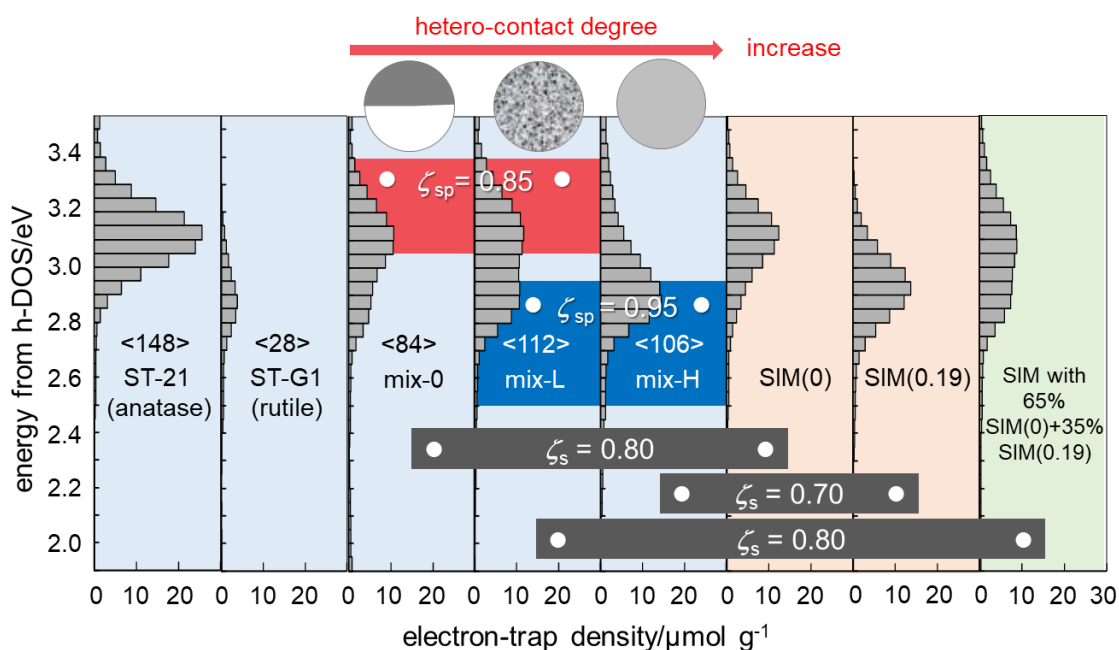


Fig. 2-5 ERDT patterns of ST-21, ST-G1 and their 50/50 mixtures prepared by different production methods, simulation patterns with energy shift of 0 eV and 0.19 eV, and summation pattern with SIM(0) and SIM(0.19) to reproduce the ERDT pattern of mix-L. ζ_{sp} represents the degrees of coincidence of shape in the red and blue energy ranges. The numbers in < > indicate total ET density. The orange/green and blue colors in the background are simulation and experimental patterns, respectively.

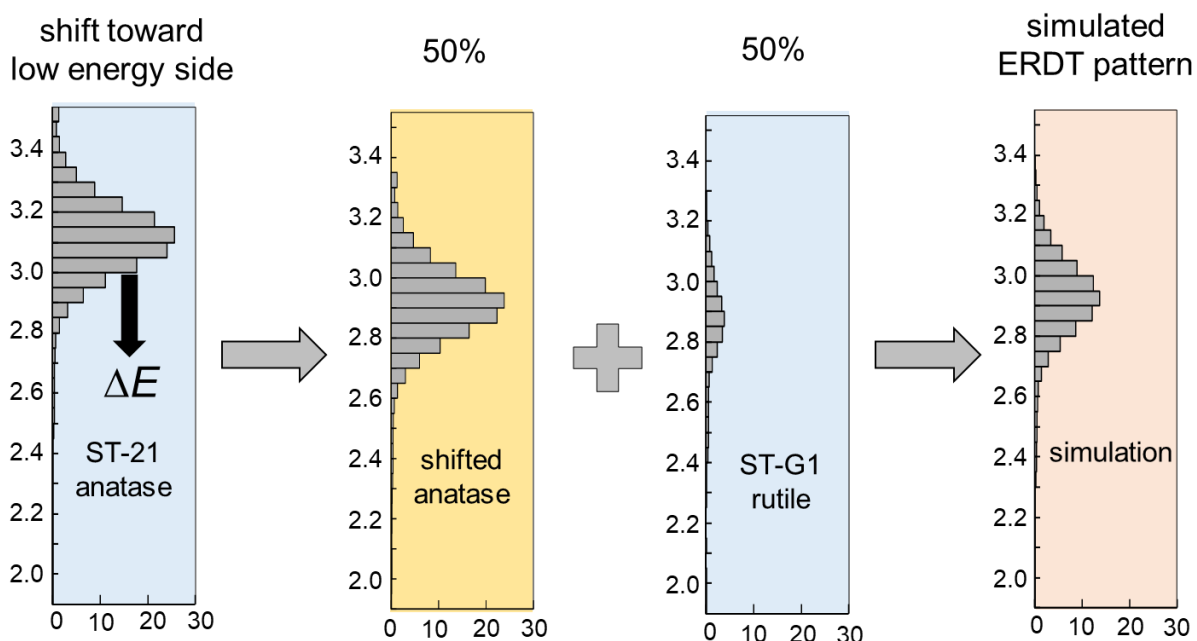


Fig. 2-6 Simulated ERDT patterns of 50/50 mixture for anatase ST-21 and rutile ST-G1.

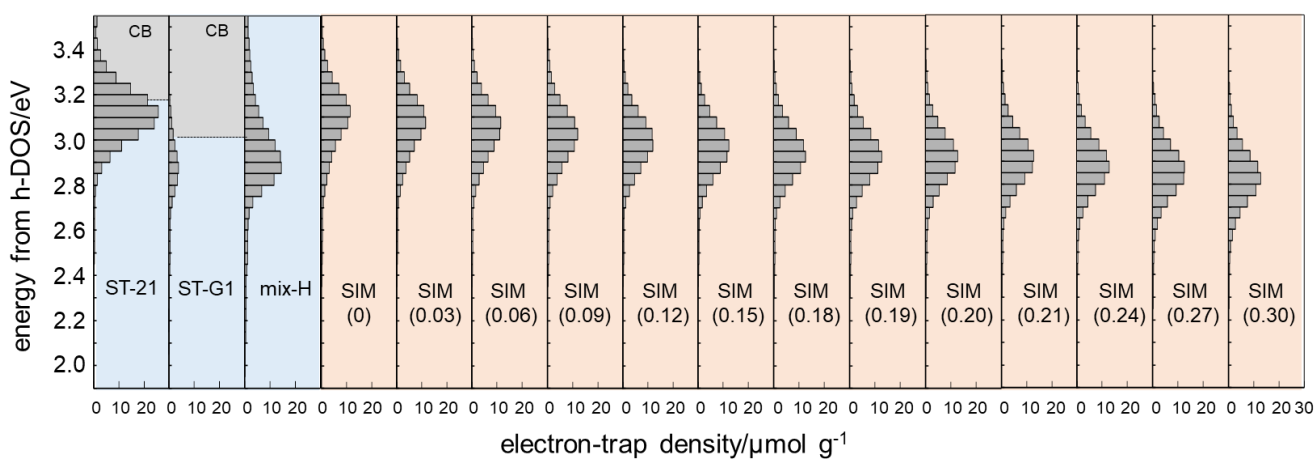


Fig. 2-7 ERDT patterns of ST-21, ST-G1, and 50/50 mixture prepared by mix-H, and simulation patterns with energy shift from 0–0.30 eV. Blue and orange colors in the background indicate experimental and simulation patterns, respectively.

2.3.2 Simulation of Energy-Resolved Distribution of Electron Traps

One of the possible reasons for the shift of ERDT patterns of mixture samples is the difference of h-DOS(VB) of original samples, and interparticle charge-transfer excitation (ICTE) occurs from the h-DOS(VB) of ST-G1 (located slightly higher than that of ST-21) to ETs in ST-21. In order to investigate this assumption, ζ_s ($0 < \zeta_s < 1$) which represent the degree of coincidence of ERDT pattern shape was proposed and the simulation was performed by shifting the original ERDT pattern to low energy side with a 0.01 eV pitch, ζ_s with the measurement one was calculated and selected the maximum one as the simulation result. As shown in Fig. 2-6, simulated ERDT patterns were prepared by summing up 50% lower-energy shifted (0–0.30 eV, 0.01-eV step) ERDT pattern of ST-21 and 50% measured ERDT pattern of ST-G1(no shift). Fig. 2-7 shows the ERDT patterns of ST-21, ST-G1, their 50/50 mixture prepared by mix-H, and simulation patterns with energy shift from 0–0.30 eV, orange and blue colors in the background indicate simulation and as-measured patterns, respectively. It can be seen that with increase in the energy shift (ΔE), the peak of simulated ERDT pattern shifted lower energy side. Calculations of ζ_s with these simulated ERDT patterns and as-measured ERDT pattern of mix-H are shown in Fig. 2-8, the energy shift degree giving the highest ζ_s was selected as ΔE_{\max} . For the 50/50 mixture of ST-21 and ST-G1, it can be seen that with increase in the energy shift (ΔE), ζ_s also increased up to 0.70 at the energy shift of 0.19 eV, then decreased with increase in the energy shift degree (ΔE), this means that the measured ERDT pattern could be reproduced by assuming all the electrons accumulated in ETs of ST-21 were excited from h-DOS(VB) of ST-G1 being 0.19 eV higher than that of ST-21.

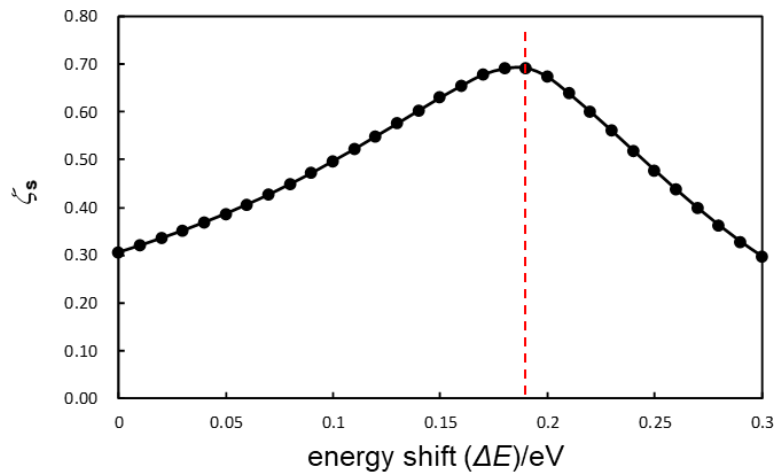


Fig. 2-8 Energy shift (ΔE) and degree of coincidence of the ERDT patterns (ζ_s) for ST-21 and ST-G1 50/50 mixtures prepared by mix-H.

It can also be seen from Fig. 2-5 that mix-L which prepared by mixed ST-21 and ST-G1 with a Teflon spatula manually for 20 min shown an interesting ERDT pattern seems to be spliced by two ERDT patterns. The ERDT pattern in energy range of 3.05 - 3.4 eV (red color energy ranges) for mix-L was similar to the ERDT pattern of same part for mix-L with a $\zeta_{sp} = 0.85$, meanwhile the ERDT pattern in energy range of 2.5 – 2.95 eV (blue color energy ranges) for mix-L was similar to the ERDT pattern of same part for mix-H with a $\zeta_{sp} = 0.95$. The difference between mix-L and mix-H is only the mixing procedures, it is easily expected that ST-21 and ST-G1 particles in mix-H were thoroughly mixed and in sufficient contact with each other compared to the particles in mix-L. Thus, the interesting ERDT pattern of mix-L might be attributed to inadequate mixing and contact between ST-21 and ST-G1 particles. Part ST-21 and ST-G1 particles in mix-L were sufficiently contacted and the ERDT pattern appears similar to mix-H, the other ST-21 and ST-G1 particles were separated and shown a ERDT pattern similar to mix-0.

2.3.3 *Interparticle Charge-Transfer Excitation*

In order to investigate this hypothesis, simulation was performed by summation of the $(100-X)\%$ ERDT pattern of SIM(0) and $X\%$ ERDT pattern of SIM(0.19), and ζ_s values between those simulated ERDT patterns and the ERDT pattern of the 50/50 mixture prepared by mix-L were calculated and selected the maximum one as the simulation result (for details, see 4.3.1). Interestingly, when $X = 35$ the maximum ζ_s was 0.80, a relatively high value. In other words, the ERDT pattern of mix-L could be reproduced by simple summation of 65% SIM(0) and 35% SIM(0.19) with ζ_s of 0.80. Therefore, the interesting ERDT pattern of mix-L might be due to the presence of two kinds of anatase particles, with and without electronic contact with rutile particles, in 35% and 65% composition. In other words, ERDT analysis provides quantitative measurement of "hetero-contact degree" (how much proportion of one kind of particles (anatase in this study) are electronically contacted with the other kind of particles (rutile in this study)).

In RDB-PAS measurement, the electrons in the VB of metal oxide samples are directly excited to and accumulated in the ETs from the lower energy side without recombination with positive holes, since irradiated continuous light (Excitation light) was scanned from longer wavelength (lower energy side) and the measurement was conducted under nitrogen saturated with methanol, which capture positive holes by donating electron to titania[Nitta 2016/ Nitta 2018]. Generally, the electron excitation model in mixture sample is considered as a respective electron excitation which the electrons in VB of mixture components excited to their own ETs from VB of themselves respectively.

However, this excitation concept cannot explain the above-mentioned results. As this concept, whether the particles of ST-21 and ST-G1 sufficiently contacted or not, the electrons in VB of ST-21 and ST-G1 were directly excited to ETs separately, there was no electronic interaction and the ERDT patterns of mixtures prepared by different mixing procedures will be similar and can be reproduced by simple summation of ERDT patterns of ST-21 and ST-G1.

Here I proposed a novel concept as a possible explanation for the above-mentioned results is interparticle charge-transfer excitation from h-DOS(VB) of the higher-h-DOS(VB) sample to ETs of both samples. As shown in Fig. 2-9, when two kinds of particles were adjoined with each other, an orbital overlap occurs between the two particles. In the overlapping orbital, photoexcitation from a higher-h-DOS(VB) sample (ST-G1, rutile) to all ETs in both particles (VB-ET) occurs, prior to photoexcitation from a lower-h-DOS(VB) sample (anatase) to ETs in a lower-h-DOS(VB) sample (anatase). The electrons of the higher-h-DOS(VB) sample (ST-G1, rutile) excitation from its h-DOS(VB) position to ETs of the lower-h-DOS(VB) sample (ST-21, anatase), excitation from the higher-h-DOS(VB) position means the VB-ET transition energy will be smaller. The smaller VB-ET transition energy means the electrons from the higher-h-DOS(VB) sample (ST-G1, rutile) can fill the ETs of the lower-h-DOS(VB) sample (ST-21, anatase) first, and the electron-filled ETs no longer accept electrons, so electrons excitation from h-DOS(VB) position of the lower-h-DOS(VB) sample (ST-21, anatase) to ETs of the lower h-DOS(VB) sample (ST-21, anatase) will not occur. The VB-ET excitation needs lower energy, resulting in a lower energy shift in the ERDT pattern of the mixture. The energy shift observed with the mixed sample might be due to the actual energy difference between the h-DOS (VB)s of anatase and rutile.

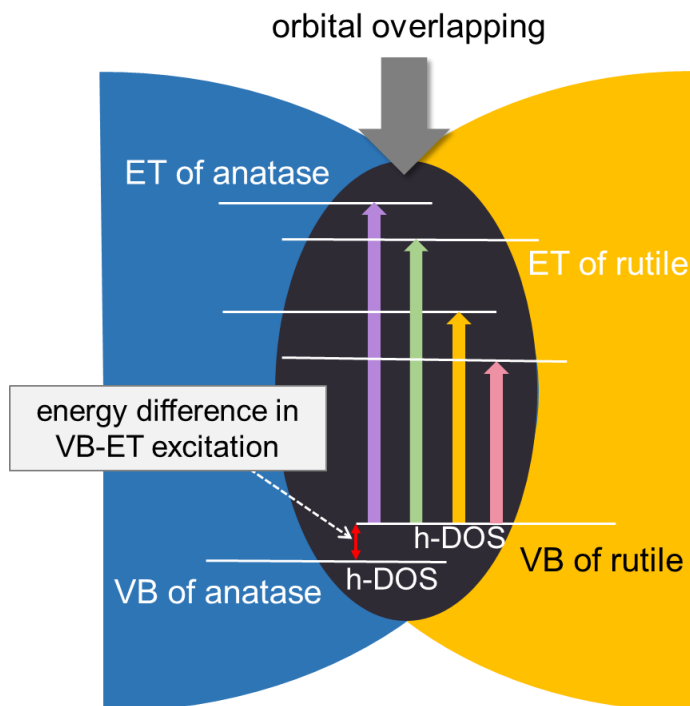


Fig. 2-9 Interparticle charge-transfer excitation from the h-DOS(VB) of a higher-h-DOS(VB) sample to all ETs in a mixture sample adjoined to make orbitals overlapped.

2.4 Conclusions

In this chapter, mixture samples of anatase and rutile prepared by different mixing methods were characterized by RDB-PAS and found that their ERDT patterns were completely different. The ERDT pattern of mix-H which prepared by braying in an agate mortar for 10 min has a shift to lower energy side compared to the simple summation of ST-21 and ST-G1 which was completely different from the mix-0 which was just put two original samples half to half on the sample holder. This is the first experimental evidence of interparticle spatial overlapping of orbitals to result in interparticle charge-transfer excitation (ICTE), i.e., photoexcitation from the h-DOS(VB) of the higher h-DOS(VB) sample to all ETs at an anatase-rutile interface. The detail energy-resolved distribution of electron traps (ERDT) analyses of anatase-rutile mixtures prepared by different mixing methods revealed that all of the photoexcitation occurred from h-DOS in valence band of rutile in thoroughly mixed sample and h-DOS of rutile was located ca. 0.19 eV higher than that of anatase. In addition, the ICTE analysis suggested a new concept, hetero-contact degree, which could be quantitatively evaluated by comparison of ERDT patterns of mixture sample to simulation patterns with thoroughly adjoined mixture particles and

non-contacted particles.

2.5 References

Fujishima 2000 Fujishima A, Rao T N, Tryk D A. Titanium dioxide photocatalysis[J]. *Journal of photochemistry and photobiology C: Photochemistry reviews*, **2000**, 1(1): 1-21.

Hoffmann 1995 Hoffmann M R, Martin S T, Choi W, et al. Environmental applications of semiconductor photocatalysis[J]. *Chemical reviews*, **1995**, 95(1): 69-96.

Shiraishi 2008 Shiraishi Y, Hirai T. Selective organic transformations on titanium oxide-based photocatalysts[J]. *Journal of Photochemistry and Photobiology C: Photochemistry Reviews*, **2008**, 9(4): 157-170.

Bickley 1991 Bickley R I, Gonzalez-Carreno T, Lees J S, et al. A structural investigation of titanium dioxide photocatalysts[J]. *Journal of Solid state chemistry*, **1991**, 92(1): 178-190.

Kamat 1993 Kamat P V. Photochemistry on nonreactive and reactive (semiconductor) surfaces[J]. *Chemical Reviews*, **1993**, 93(1): 267-300.

Hurum 2003 Hurum D C, Agrios A G, Gray K A, et al. Explaining the enhanced photocatalytic activity of Degussa P25 mixed-phase TiO₂ using EPR[J]. *The Journal of Physical Chemistry B*, **2003**, 107(19): 4545-4549.

Ohno 2003 Ohno T, Tokieda K, Higashida S, et al. Synergism between rutile and anatase TiO₂ particles in photocatalytic oxidation of naphthalene[J]. *Applied Catalysis A: General*, **2003**, 244(2): 383-391.

Sun 2018 Sun X, Chang Y, Cheng Y, et al. Band alignment-driven oxidative injury to the skin by anatase/rutile mixed-phase titanium dioxide nanoparticles under sunlight exposure[J]. *Toxicological Sciences*, **2018**, 164(1): 300-312.

Creutz 2005 Creutz C, Brunschwig B S, Sutin N. Interfacial charge-transfer absorption: semiclassical treatment[J]. *The Journal of Physical Chemistry B*, **2005**, 109(20): 10251-10260.

Irie 2008 Irie H, Miura S, Kamiya K, et al. Efficient visible light-sensitive photocatalysts: grafting Cu (II) ions onto TiO₂ and WO₃ photocatalysts[J]. *Chemical Physics Letters*, **2008**, 457(1-3): 202-205.

Irie 2009 Irie H, Kamiya K, Shibamura T, et al. Visible light-sensitive Cu (II)-grafted TiO₂ photocatalysts: activities and X-ray absorption fine structure analyses[J]. *The Journal of Physical Chemistry C*, **2009**, 113(24): 10761-10766.

Yu 2010 Yu H, Irie H, Hashimoto K. Conduction band energy level control of titanium dioxide: toward an efficient visible-light-sensitive photocatalyst[J]. *Journal of the American Chemical Society*, **2010**, 132(20): 6898-6899.

Nitta 2016 Nitta A, Takase M, Takashima M, et al. A fingerprint of metal-oxide powders: energy-resolved distribution of electron traps[J]. *Chemical Communications*, **2016**, 52(81): 12096-12099.

Nitta 2019 Nitta A, Takashima M, Takase M, et al. Identification and characterization of titania photocatalyst powders using their energy-resolved distribution of electron traps as a fingerprint[J]. *Catalysis Today*, **2019**, 321: 2-8.

Nitta 2018 Nitta A, Takashima M, Murakami N, et al. Reversed double-beam photoacoustic spectroscopy of metal-oxide powders for estimation of their energy-resolved distribution of electron traps and electronic-band structure[J]. *Electrochimica acta*, **2018**, 264: 83-90.

Buchalska 2015 Buchalska M, Kobielusz M, Matuszek A, et al. On oxygen activation at rutile-and anatase-TiO₂[J]. *ACS Catalysis*, **2015**, 5(12): 7424-7431.

Shen 2020 Shen Y, Nitta A, Takashima M, et al. Do Particles Interact Electronically?—Proof of Interparticle Charge-Transfer Excitation between Adjoined Anatase and Rutile Particles[J]. *Chemistry Letters*, **2020**, 49(X).

Ikeda 2003 Ikeda S, Sugiyama N, Murakami S, et al. Quantitative analysis of defective sites in titanium (IV) oxide photocatalyst powders[J]. *Physical Chemistry Chemical Physics*, **2003**, 5(4): 778-783.

Evaluation of Relative Band Structure of Semiconducting Metal Oxides

3.1 Introduction

Titanium(IV) oxide (titania), the most widely used metal oxide for photocatalytic applications [Fujishima 2000/Hoffmann 1995/Shiraishi 2008], is categorized into semiconductor based on its electronic energy structure and the band structure composed of an electron-filled valence band (VB), electron-vacant conduction band (CB) and forbidden band (bandgap) separating them from each other, though it seems the real band structure of titania and the other metal oxides is still speculative and only conduction-band bottom (CBB) and valence-band top (VBT) positions have been discussed mainly. The bandgaps of anatase and rutile are ca. 3.2 eV [Tang 1993] and 3.0 eV [Minoura 1985] respectively have been reported. Researchers also studied the conduction-band bottom (CBB) and valence-band top (VBT) positions of anatase and rutile through materials simulation techniques [Scanlon 2013/Zhang 2014]. However, the higher density of states (DOS) part of the VB (h-DOS(VB)), which causes actual photoabsorption of materials is still lack of understanding. Here, a novel method has been developed for identification and detailed characterization of metal-oxide powders with energy-resolved distribution of electron traps (ERDT) measured by reversed double-beam photoacoustic spectroscopy (RDB-PAS) [Nitta 2016/Nitta 2019/Nitta 2018/Buchalska 2015]. In this study, ERDT patterns of metal oxides mixtures were measured and analyzed to elucidate the actual band position of semiconducting metal oxides such as titania [Shen 2020].

3.2 Experimental

3.2.1 Materials

Commercial metal oxide samples, laboratory-made octahedral shape anatase particle (OAP) [Amano 2009] and samples from Japan Reference Catalyst (JRC-TiO series) supplied by the Catalysis Society of Japan (CSJ) was used, their properties are shown in Table 3-1. The details of mix-0, mix-L and mix-H are described in 2.2.1.

Since the P25 sample is highly heterogeneous, and sampling it will result in receiving various data about its composition (anatase rutile and amorphous), first the P25 sample (AEROXIDE®TiO₂ P25 produced by Japan Aerosil Co., Ltd) need to be homogenize. 20 g of P25 powder was suspended in 0.2 L Milli-Q water and stirred for 24

h, then freeze-dried for 24 h (<193 K, <10 Pa) to obtain the HomoP25. 6 g of HomoP25 was suspended in a mixture of 200 mL hydrogen peroxide (30%) and 6 mL ammonia (25%), mechanically stirred for 15 h at 298 K, washed with water, then freeze-dried and aerobic annealed for 2.5 h at 473 K to obtain the isolated-anatase (ANA) sample. The isolated-rutile (RUT) sample was obtained from 9 g of HomoP25 was suspended in 200 mL aqueous solution of hydrofluoric acid (10%), mechanically stirred for 15 h, washed with water and alkaline solution (NaOH, 1 g/mol), then freeze-dried and aerobic annealed for 2.5 h at 473 K [Wang 2018].

3.2.2 Photoacoustic Spectroscopy (PAS) and Reversed Double-beam Photoacoustic Spectroscopy (RDB-PAS) Measurement

The details are described in 2.2.2.

3.2.3 Photoelectron Yield Spectroscopic (PYS) Measurement

The photoelectron yield spectroscopic were measured by BIP-KV201 (Bunkoiki) in an air atmosphere. Ionization energy was estimated from threshold value of photoelectron yield spectrum which was one-third power of yield as a function of photon energy.

3.3 Results and Discussion

3.3.1 Maximum Energy Shift (ΔE_{max}) Values of 50/50 Mixtures of Different Kinds of Titania

In Chapter 2, the interparticle charge-transfer excitation (ICTE), that is photoexcitation from the h-DOS(VB) of the higher h-DOS(VB) sample (rutile) to all ETs at an anatase-rutile interface has been discussed. The detail ERDT analyses of various anatase-rutile mixtures suggest that all of the photoexcitation occurred from h-DOS in valence band of rutile sample in thoroughly mixed sample and h-DOS of rutile was located ca. 0.19 eV higher than that of anatase. For further analysis, I tried characterize different kinds of titania and their mixtures prepared as mix-H with RDB-PAS to analysis the energy shift (ΔE) of different kinds of titania samples (In this study, I use commercial metal oxide samples, laboratory-made octahedral shape anatase (OAP) and samples from

Japan Reference Catalyst (JRC-TIO series) supplied by the Catalysis Society of Japan (CSJ), their properties are shown in Table 3-1.).

Table 3-1 Structural and bulk properties of samples used in this study.

sample name	supplier ^a	crystalline composition ^b (%)			SSA ^c / m ² g ⁻¹	crystallite size ^d /nm
		anatase	rutile	non-crystal		
OAP	(laboratory-made)	97	0	3	21	80
PC-102	Titan	91	0	9	157	12
ST-01	Ishihara	80	0	20	344	8
ST-157	Ishihara	81	0	19	81	15
ST-21	Ishihara	87	0	13	67	25
TIO-1	CSJ (Ishihara)	91	0	9	79	21
CR-EL	Ishihara	1	94	4	8	200
HT-0514	Toho	1	94	5	7	—
MT-150A	Tayca	0	82	18	114	—
ST-G1	Showa	0	97	3	7	250
TIO-3	CSJ (Ishihara)	0	90	10	47	40
CeO ₂	Kanto	—	—	—	10	552
WO ₃	Kojundo	—	—	—	6	595

^aTitan: Titan Kogyo, Ishihara: Ishihara Sangyo, CSJ: Catalysis Society of Japan, Toho: Toho Titanium, Showa: Showa Denko Ceramics, Kanto: Kanto Chemical, Kojundo: Kojundo Chemical Laboratory. ^bObtained from Rietveld analysis measured by a Rigaku SmartLab X-ray diffractometer with 20wt% nickel(II) oxide to calculate non-crystalline content.⁶ Since each composition was rounded, total composition might not be 100%. ^cSpecific surface area estimated by Brunauer-Emmett-Teller (BET) equation from nitrogen adsorption amount measured with Quantachrome Autosorb-6 at 77 K. ^dEstimated by Scherrer equation with corresponding peak width from XRD analyses.

As shown in Table 3-2, ΔE_{\max} values for the mixtures with anatase and rutile except for the mixture with TIO-1 and MT-150A were 0.18–0.19 eV, suggesting that the h-DOS(VB) of anatase except for TIO-1 were lower than that of rutile by ca. 0.19 eV and that photoexcitation from rutile h-DOS(VB) to anatase ETs might occur in the mixture sample, which is the first experimental results proving overlap of orbitals. On the other hand, the ERDT pattern of mixture of anatase and anatase, rutile and rutile can be reproduced by simple summation (simulation with $\Delta E = 0$) by ERDT pattern of original samples, ΔE_{\max} for the mixtures with two anatase samples and two rutile samples was negligible, indicate that energy differences between the h-DOS(VB)s of two anatase samples and two rutile samples were negligible. These results suggest the assumption that ΔE_{\max} reflects the h-DOS(VB) energy difference as the bulk electronic structure, not surface structure, difference. The reason why ΔE_{\max} values of the mixtures including TIO-1 and MT-150A were 0.12–0.13 eV will be discussed in 3.3.3.

Table 3-2 Maximum energy-shift (ΔE_{\max}) values of 50/50 mixtures of different kinds of titania samples prepared as mix-H. Green and blue cells indicate anatase and rutile, respectively.

sample 1	sample 2	$\Delta E_{\max}/\text{eV}$
OAP	CR-EL	0.17
OAP	HT-0514	0.18
OAP	ST-G1	0.18
PC-102	ST-G1	0.19
PC-101	CR-EL	0.18
ST-01	ST-G1	0.19
ST-01	HT-0514	0.18
ST-01	CR-EL	0.18
ST-157	ST-G1	0.18
ST-157	CR-EL	0.19
ST-21	HT-0514	0.18
ST-21	ST-G1	0.19
ST-21	CR-EL	0.19
ST-21	TIO-3	0.18
ST-01	MT-150A	0.13
ST-21	MT-150A	0.12
TIO-1	TIO-3	0.13
ST-01	ST-21	0.00
ST-01	ST-157	0.00
HT-0514	ST-G1	0.01
HT-0514	CR-EL	0.00

3.3.2 Maximum Energy Shift (ΔE_{\max}) Values of Different Anatase Contents in Mixtures

The ΔE_{\max} dependence on anatase content in the mixtures prepared by mix-H was examined. As shown in Fig. 3-1, ΔE_{\max} values of mixtures prepared by ST-21 and ST-G1 were constant until the anatase ratio of 0.6 and then decreased with increase in the rutile content. It is easy to expect that with lower anatase content, almost all of the anatase (ST-21) particles were in sufficient contact with rutile (ST-G1) particles, while at a higher

anatase content, not all of the anatase (ST-21) particles had sufficient contact with rutile (ST-G1) particles, this will cause the ERDT pattern of mixture to appear a peak in the high energy region will resulting in the decrease in observed ΔE_{\max} , the details will be discussed in 4.3.3. It can be seen from the other combinations, the inflection points of the anatase ratio increased with decrease in the ratio of crystallite sizes of anatase sample and rutile sample, most probably because relatively small anatase particles could easily make contact with large rutile particles. In addition, it can be seen that the constant ΔE_{\max} which

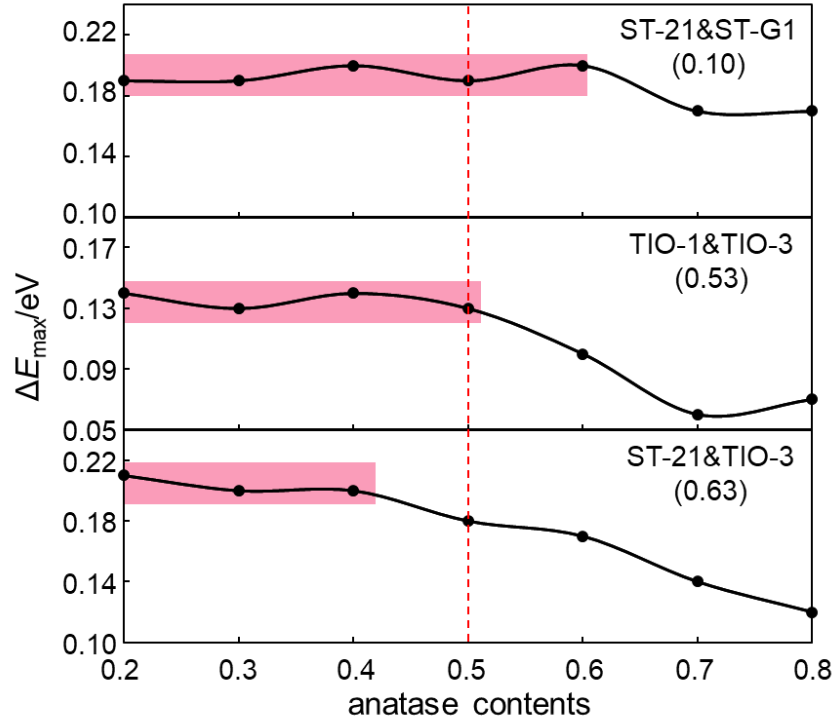


Fig. 3-1 Maximum energy shift (ΔE_{\max}) as a function of anatase content in mixtures prepared as mix-H. The numbers in () denote the crystallite size ratio of anatase and rutile calculated from XRD peak width.

was ca. 0.2 eV, might be the actual energy difference between h-DOS(VB) position of anatase and rutile. The above results indicate that ERDT analysis can be used to estimate the actual difference of h-DOS (VB) position in mixture samples with different h-DOS(VB)s and this is the first experimental measurements of practical h-DOS(VB) energy.

3.3.3 Evaluation of the Relative Band Structure of Titania

As discussed in 3.3.1 and 3.3.2, energy shift (ΔE_{\max}) obtained from ERDT pattern of mixture sample prepared by mix-H may indicated the h-DOS(VB) energy difference of

the original samples. Meanwhile, the ionization energy (I_p) of samples were estimated from photoelectron yield spectroscopy. Table 3-3 shows the bulk composition obtained from the XRD measurement, bandgap estimated by PAS, ionization energy difference and h-DOS(VB) energy difference of ST-21 and ST-G1. It can be seen in Table 3-3 that the ΔI_p and ΔE_{\max} of ST-21 and ST-G1 were clearly different. Ionization energy is a leading energy parameter of semiconductors, which is defined as the minimum energy for removing the electron from the system [Toyoda 2015]. The threshold of photoelectron emission which is the minimum energy required for electrons to emitted from the solid surface by UV irradiation was regarded as the VBT position of n-type metal oxide semiconductors. On the other hand, as discussed in 2.1.1, in RDB-PAS measurement electrons directly excited to ETs may occur from the h-DOS(VB) not the VBT. Regarded h-DOS(VB) as apparent VBT, the above-mentioned results may suggest that ΔE_{\max} correspond to energy difference of apparent VBT which located lower than VBT was the energy level which electrons directly excitation occur. Therefore, the difference of ΔI_p and ΔE_{\max} of ST-21 and ST-G1 might be the energy difference of apparent VBT and VBT.

I have obtained bandgap from PAS measurement, added ΔI_p and ΔE_{\max} , these results may be used to estimation of relative band structure of metal-oxide samples. As shown in Table 3-3, bandgap of ST-21 and ST-G1 were 3.2 eV and 2.99 eV, the ΔI_p and ΔE_{\max} of ST-21 and ST-G1 were 0.04 eV and 0.19 eV. On the basis of these results, the band structure of ST-21 and ST-G1 might be estimated as shown in Fig. 3-2, the h-DOS(VB) position which located lower than VBT of ST-21 was 0.19 eV lower than ST-G1 and the VBT of ST-21 was 0.04 eV lower than ST-G1, then basis of the bandgap of two samples, the CBB of ST-21 was 0.17 eV higher than ST-G1. The absorption spectrum of ST-21(anatase) and ST-G1 (rutile) measured by photoacoustic spectroscopy (PAS) were shown in Fig. 3-3. It can be seen from the figure that consistent with the well known observation that the rise at photoabsorption edge of rutile (blue frame) is steeper than that of anatase (red frame), this suggest that the difference between VBT and h-DOS(VB) for rutile is smaller than that for anatase. This is consistent with the above mentioned relative band structure of ST-21(anatase) and ST-G1 (rutile).

Table 3-3 Bulk composition, CBB, ionization energy difference and apparent VBT energy difference of ST-21 and ST-G1.

sample	composition (%)		E_{CBB}/eV	$I_{\text{p}}^{\text{a}}/\text{eV}$	$\Delta I_{\text{p}}^{\text{b}}/\text{eV}$	$\Delta E_{\text{max}}/\text{eV}$
	anatase	rutile				
ST-21	87	0	3.2	7.35	0.04	0.19
ST-G1	0	97	2.99	7.31		

^aIonization energy, ^benergy difference of I_{p} between ST-21 and ST-G1, ^cenergy difference h-DOS(VB) position measured by RDB-PAS.

Not only anatase and rutile, I also examined the band structure of amorphous sample. Fig. 3-4 shows the ERDT pattern of amorphous, HT-0514 (rutile), their mixture and the simulation result. The simulation was performed by summing up 50% lower-energy shifted (0–0.30 eV, 0.01-eV step) ERDT pattern of amorphous sample and 50% measured ERDT pattern of HT-0514 (rutile), the ζ_{s} with the measurement one was calculated and selected the highest one as the simulation result. It can be seen from the figure that the energy shift (ΔE_{max}) of mix-H prepared by amorphous and HT-0514 is 0.52 eV. This may suggest the h-DOS(VB) of amorphous is 0.52 eV higher than that of HT-0514 (rutile).

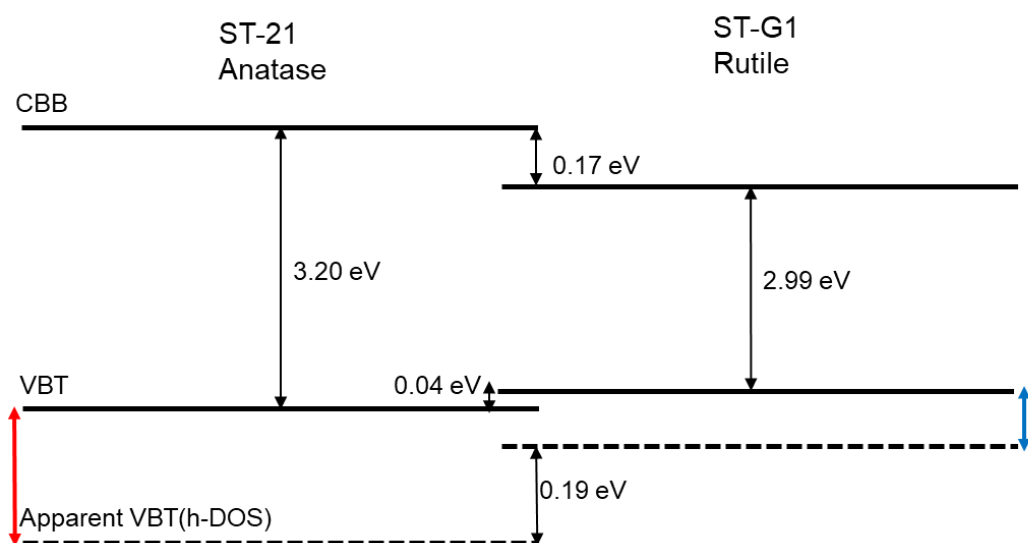


Fig. 3-2 Estimation of band structure of ST-21 and ST-G1 through energy-resolved distribution of electron traps.

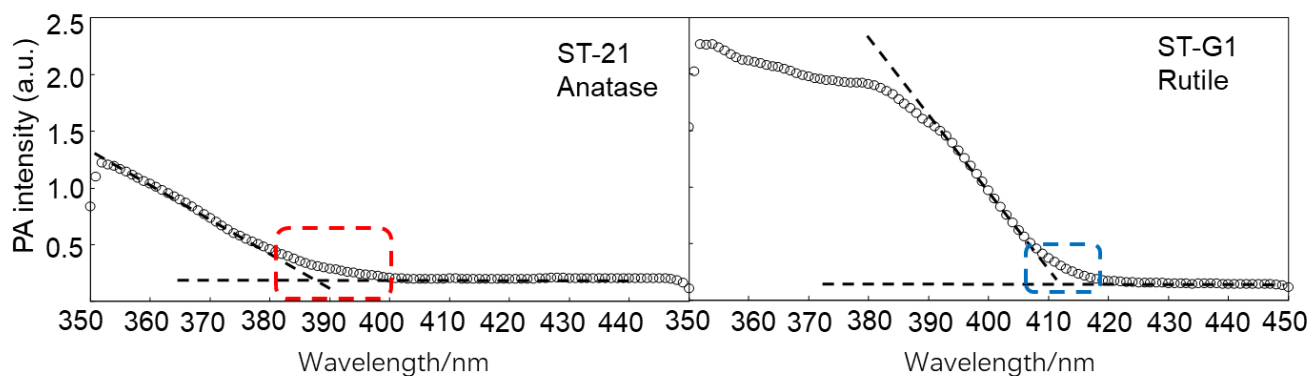


Fig. 3-3 Rise at photoabsorption edge of rutile (blue frame) is steeper than that of anatase (red frame), energy difference between VBT and h-DOS(VB) for rutile is smaller than that for anatase.

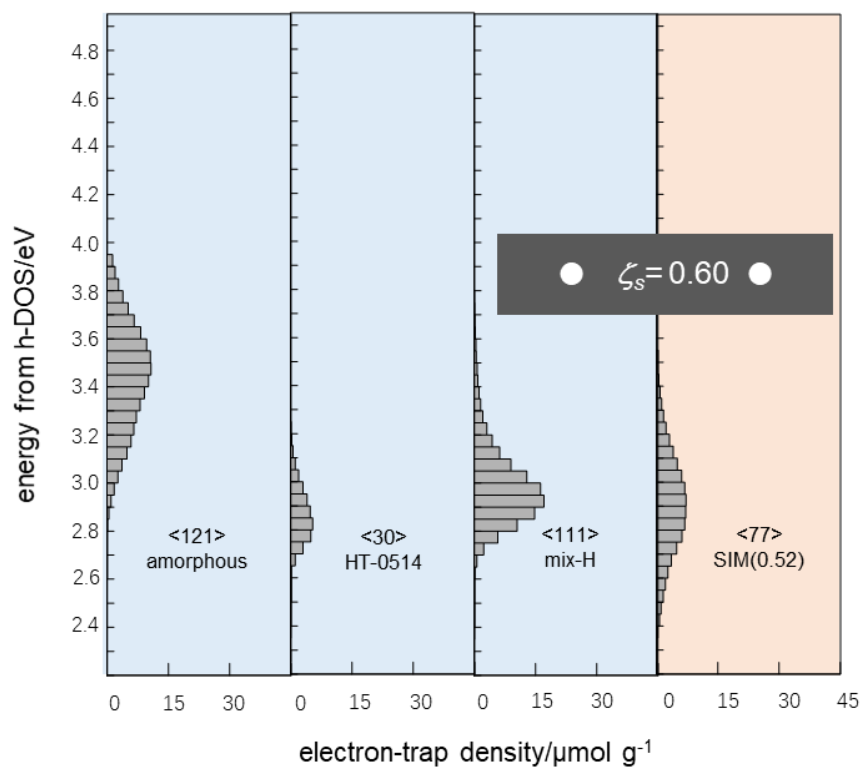


Fig. 3-4 ERDT patterns of amorphous, HT-0514 (rutile), their 50/50 mixtures prepared by mix-H, simulation patterns with energy shift of 0.52 eV. The numbers in < > indicate total ET density. The orange and blue colors in the background are simulation and experimental patterns, respectively.

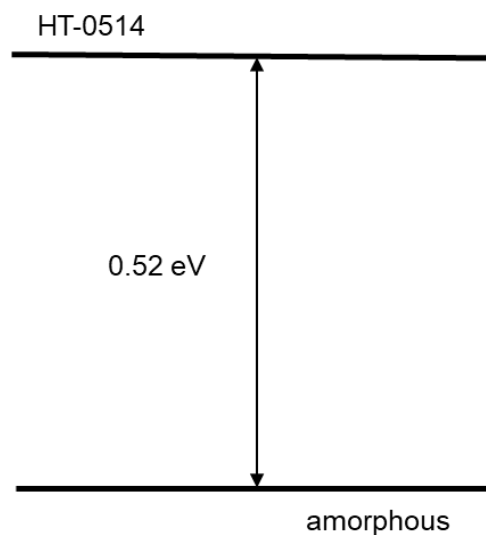


Fig. 3-5 Estimation of band structure of amorphous and HT-0514 (rutile) through energy-resolved distribution of electron traps.

In 3.3.2, I discussed the ΔE_{\max} values of the mixtures including TIO-1 and MT-150A found that they were different with the other anatase and rutile samples. For further research, the mixtures of TIO-1, MT-150A with other commercial titania samples were characterized by reversed double-beam photoacoustic spectroscopy (RDB-PAS) to elucidate their actual position of h-DOS(VB).

Fig. 3-6 shows the ERDT patterns of TIO-1(anatase), HT-0514(rutile), ST-21(anatase) and their mixtures. The simulation was performed by shifting the original ERDT pattern to low energy side with a 0.01 eV pitch, the ζ_s with the measurement one was calculated and selected the highest one as the simulation result (for details, see 2.3.2). It can be seen from the figure that the ΔE_{\max} of mix-H of TIO-1 and HT-0514 was 0.11 eV. At the same time ΔE_{\max} of mix-H of ST-21 and TIO-1 was 0.07 eV. This means that the h-DOS(VB) position of TIO-1 is 0.07 eV higher than ST-21 and 0.11 eV lower than HT-0514. Therefore, the h-DOS(VB) position of ST-21 should be 0.18 eV lower than HT-0514. The experimental result shows that the h-DOS(VB) position of ST-21 is 0.18 eV lower than HT-0514(see Table 3-2), consistent with the above calculation. Obviously, the ERDT pattern of TIO-1 seems shifts to the low energy side compared to other anatase samples (the peak of ERDT pattern of TIO-1 in energy located around 3.05 eV, that of other anatase samples was in energy located around 3.15 eV). The reason why ΔE_{\max} values of TIO-1 was different with the other anatase samples might be the potential of hydrogen (PH) value on the surface of TIO-1 makes the ERDT pattern of TIO-1 shift to lower energy side [Ikeda 2003].

The ERDT patterns of ST-01(anatase), HT-0514(rutile), MT-150A(rutile) and their mixtures were shown in Fig. 3-8. The simulation was performed by shifting the original ERDT pattern to low energy side with a 0.01 eV pitch, the ζ_s with the measurement one was calculated and selected the highest one as the simulation result (for details, see 2.3.2). As shown in Fig. 3-8, ΔE_{\max} of mix-H of MT-150A and HT-0514 was 0.05 eV. Simultaneously, ΔE_{\max} of mix-H of ST-01 and MT-150A was 0.07 eV. This suggest that the h-DOS(VB) position of MT-150A is 0.12 eV higher than ST-01 and 0.05 eV lower than HT-0514. Therefore, the h-DOS(VB) position of ST-01 should be 0.17 eV lower than HT-0514. It can be seen from Fig. 3-8 that ΔE_{\max} of mix-H of ST-01 and HT-0514 was 0.17 eV, this means he h-DOS(VB) position of ST-01 is 0.17 eV lower than HT-0514. The experiment result was consistent with the above calculation. Obviously, the ERDT pattern of MT-150A seems to shift to the high energy side compared to other rutile samples (the peak of ERDT pattern of MT-150A located around 2.95 eV, that of other rutile samples was in energy located around 2.80 eV).

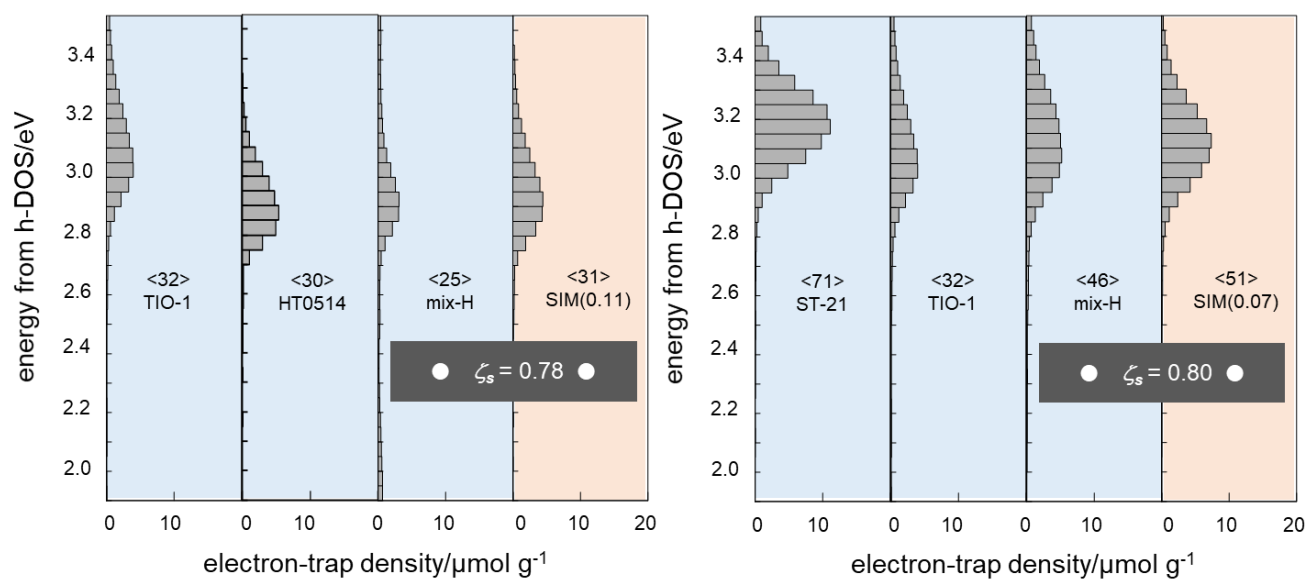


Fig. 3-6 ERDT patterns of TIO-1(anatase), HT-0514(rutile), ST-21(anatase), their 50/50 mixtures prepared by mix-H and the simulation patterns. The numbers in < > indicate total ET density. The orange and blue colors in the background are simulation and experimental patterns, respectively.

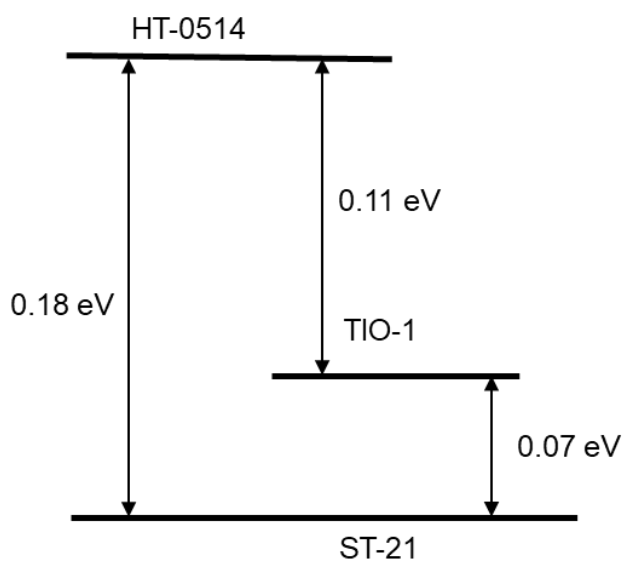


Fig. 3-7 Estimation of band structure of TIO-1(anatase), HT-0514(rutile) and ST-21(anatase) through energy-resolved distribution of electron traps.

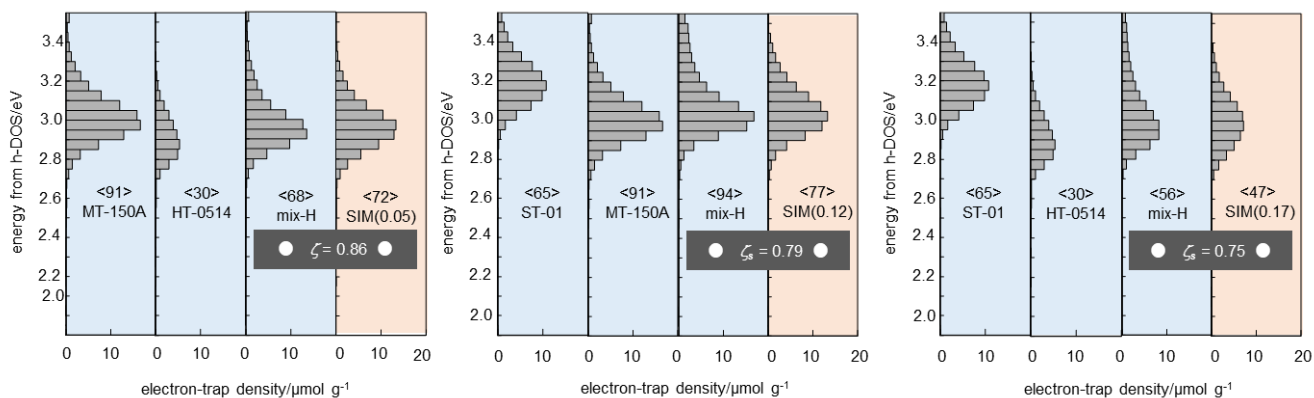


Fig. 3-8 ERDT patterns of ST-01(anatase), HT-0514(rutile), MT-150A(rutile), their 50/50 mixtures prepared by mix-H and the simulation patterns. The numbers in < > indicate total ET density. The orange and blue colors in the background are simulation and experimental patterns, respectively.

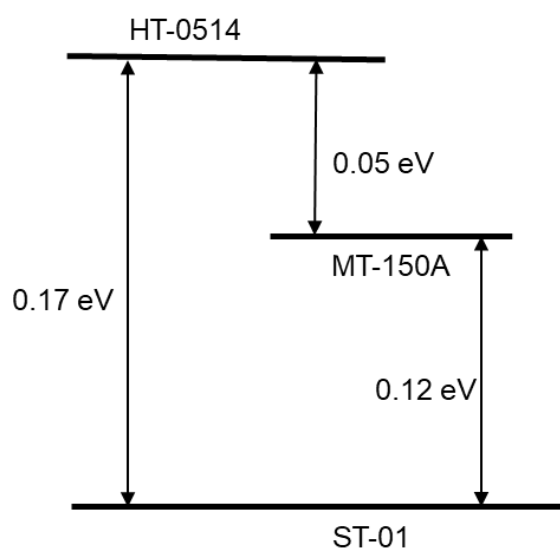


Fig. 3-9 Estimation of band structure of ST-01(anatase), HT-0514(rutile) and MT-150A(rutile) through energy-resolved distribution of electron traps.

3.3.4 Evaluation of the Band Structure of Anatase and Rutile Isolated from P25

P25 is a commercial titania sample, produced by Nippon Aerosil Co., Ltd., and composed anatase, rutile and amorphous phase. In order to study the interaction and band structure of anatase and rutile in the P25 component, the anatase particles (isolated-anatase) and rutile particles (isolated-rutile) from P25 sample were prepared by chemical dissolution method (for details, see 3.2.1). The properties of isolated-anatase (ANA), isolated-rutile (RUT) and HomoP25 are shown in Table 3-4.

The ERDT patterns of isolated-anatase (ANA), isolated-rutile (RUT), their 50/50 mixtures prepared by mix-H and the simulation patterns were shown in Fig. 3-10. The simulation was performed by summing up 50% lower-energy shifted (0–0.30 eV, 0.01-eV step) ERDT pattern of isolated-anatase (ANA) and 50% measured ERDT pattern of isolated-rutile (RUT), the ζ_s with the measurement ERDT pattern of mix-H was calculated and selected the highest one as the simulation result (for details, see 2.3.2). It can be seen from Fig. 3-10 that the ΔE_{\max} of mix-H of isolated-anatase (ANA) and isolated-rutile (RUT) is 0.05 eV with a 0.91 ζ_s . This may suggest that the h-DOS(VB) of rutile isolated from P25 is 0.05 eV higher than that of anatase isolated from P25, this is different from most commercial titania and rutile (the h-DOS(VB) of most commercial titania and rutile shown a ca. 0.2 eV energy difference).

Table 3-4 Structural and bulk properties of ANA, RUT and HomoP25 [Wang 2018].

sample	composition ^a (%)			crystallite size ^b /nm		SSA ^c / m ² g ⁻¹
	anatase	rutile	non-crystal	anatase	rutile	
HomoP25	78	14	8	25.3	39.6	52
ANA	86	1	13	23.7	—	61
RUT	0	98	2	—	39.5	28

^aObtained from Rietveld analysis measured by a Rigaku SmartLab X-ray diffractometer with 20wt% nickel(II) oxide to calculate non-crystalline content. Since each composition was rounded, total composition might not be 100%. ^bEstimated by Scherrer equation with corresponding peak width from XRD analyses. ^cSpecific surface area estimated by Brunauer-Emmett-Teller (BET) equation from nitrogen adsorption amount measured with Quantachrome Autosorb-6 at 77 K.

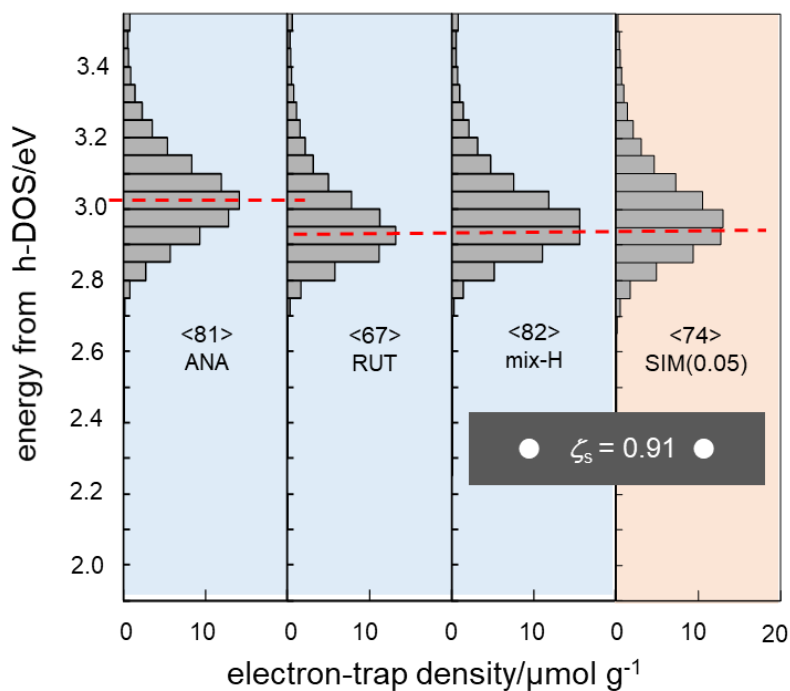


Fig. 3-10 ERDT patterns of isolated-anatase (ANA), isolated-rutile (RUT), their 50/50 mixtures prepared by mix-H and the simulation patterns. The numbers in < > indicate total ET density. The orange and blue colors in the background are simulation and experimental patterns, respectively.

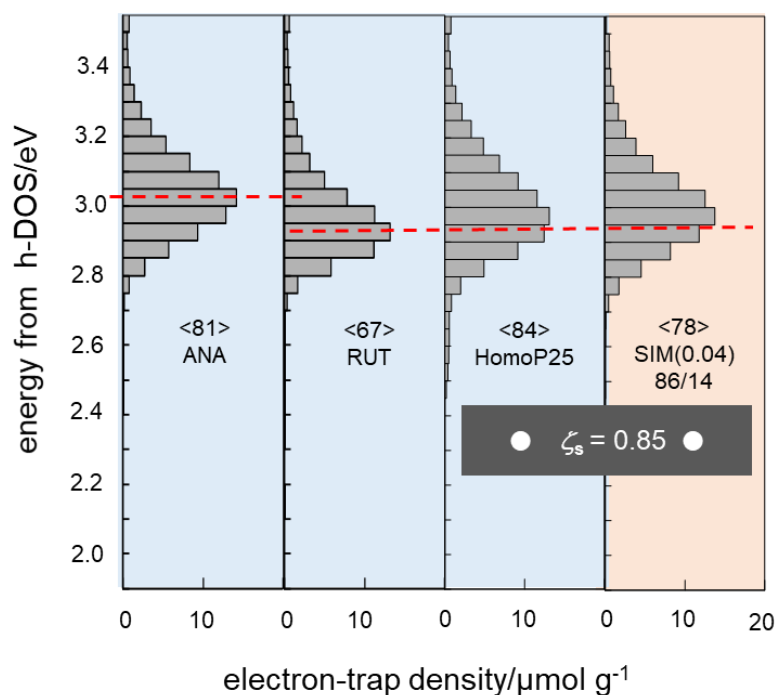


Fig. 3-11 ERDT patterns of isolated-anatase (ANA), isolated-rutile (RUT), HomoP25 and the simulation patterns. The numbers in < > indicate total ET density. The orange and blue colors in the background are simulation and experimental patterns, respectively.

For further research, I conducted a special simulation. The simulation was performed by summing up 86% (determined by the composition of anatase in HomoP25) lower-energy shifted (0–0.30 eV, 0.01-eV step) ERDT pattern of isolated-anatase (ANA) and 14% (determined by the composition of rutile in HomoP25) measured ERDT pattern of isolated-rutile (RUT), the ζ_s with the measurement ERDT pattern of HomoP25, not mix-H was calculated and selected the highest one as the simulation result (for details, see 2.3.2).

As shown in Fig. 3-11, the ΔE_{\max} of HomoP25 of isolated-anatase (ANA) and isolated-rutile (RUT) is 0.04 eV with a 0.85 ζ_s . Considering the above result shown the h-DOS(VB) of rutile isolated from P25 is 0.05 eV higher than that of anatase isolated from P25, very close to 0.04 eV. These suggest that the ERDT pattern of HomoP25 can be reproduced by summing up 86% lower-energy shifted (0.04 eV) ERDT pattern of isolated-anatase (ANA) and 14% measured ERDT pattern of isolated-rutile (RUT). In addition, the total electron traps density of SIM(0.04) was 78 $\mu\text{mol g}^{-1}$ which was almost same with HomoP25, the crystallite size of isolated-anatase (ANA) and isolated-rutile (RUT) is similar with that of anatase and rutile composition in HomoP25 (see Table 3-4). Since the ΔE_{\max} reflects the h-DOS(VB) energy difference as the bulk electronic structure, the ERDT pattern and total electron traps density reflects the surface structure and specific surface area, the crystallite size estimated by Scherrer equation with corresponding peak width from XRD analyses reflects the bulk structure. It seems that the isolated-anatase (ANA) and isolated-rutile (RUT) can be seen as the anatase and rutile composition of HomoP25, and the chemical dissolution separation process did not affect the structural and bulk properties of the anatase and rutile composition in HomoP25.

For further analysis, ΔE_{\max} values of mixtures prepared different kinds of commercial titania with isolated-anatase (ANA) and isolated-rutile (RUT) were examined. The ERDT patterns of CR-EL (rutile), isolated-anatase (ANA), isolated-rutile (RUT), their 50/50 mixtures prepared by mix-H and the simulation patterns were shown in Fig. 3-12. The simulation was performed by summing up 50% lower-energy shifted (0–0.30 eV, 0.01-eV step) ERDT pattern of isolated-anatase (ANA) / isolated-rutile (RUT) and 50% measured ERDT pattern of CR-EL (rutile), the ζ_s with the measurement ERDT pattern of mix-H was calculated and selected the highest one as the simulation result (for details, see 2.3.2). As shown in the Fig. 3-12, the ΔE_{\max} of mix-H of isolated-anatase (ANA) and CR-EL (rutile) is 0.05 eV with a 0.77 ζ_s , ΔE_{\max} of mix-H of isolated-rutile (RUT) and CR-EL (rutile) is 0 eV with a 0.72 ζ_s . This may suggest that the h-DOS(VB) of CR-EL (rutile) is 0.05 eV higher than that of anatase isolated from P25. Meanwhile, the h-DOS(VB) of CR-EL (rutile) is same with isolated-rutile (RUT).

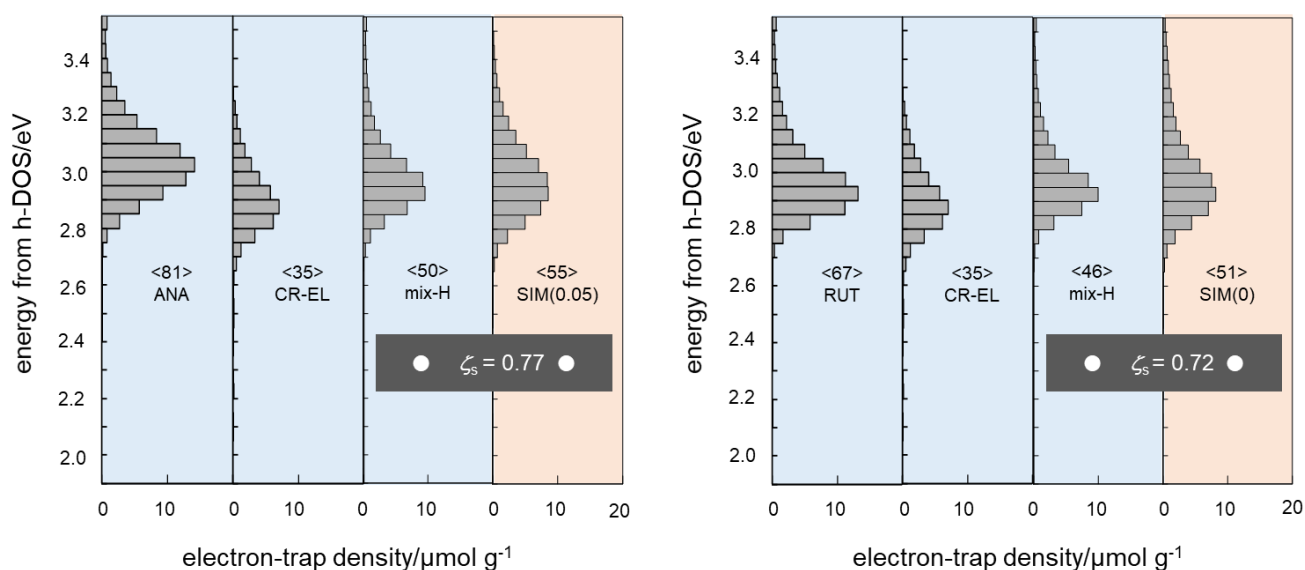


Fig. 3-12 ERDT patterns of CR-EL(rutile), isolated-anatase (ANA), isolated-rutile (RUT), their 50/50 mixtures prepared by mix-H and the simulation patterns. The numbers in < > indicate total ET density. The orange and blue colors in the background are simulation and experimental patterns, respectively.

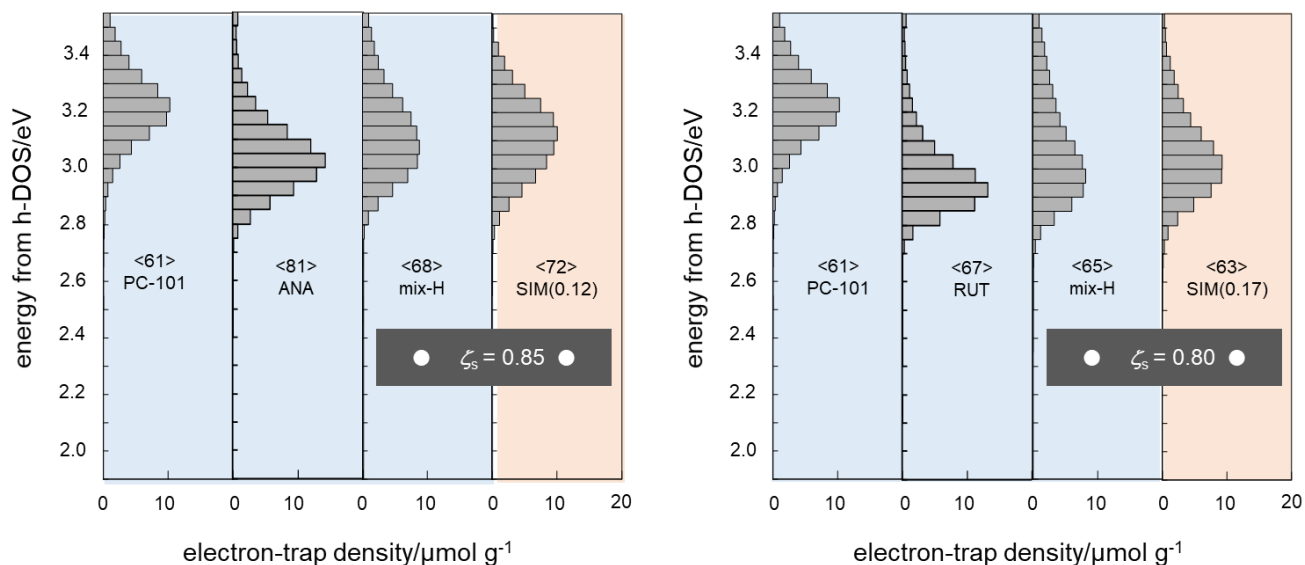


Fig. 3-13 ERDT patterns of PC-101(anatase), isolated-anatase (ANA), isolated-rutile (RUT), their 50/50 mixtures prepared by mix-H and the simulation patterns. The numbers in < > indicate total ET density. The orange and blue colors in the background are simulation and experimental patterns, respectively.

Figure. 3-13 shows the ERDT patterns of PC-101(anatase), isolated-anatase (ANA), isolated-rutile (RUT), their 50/50 mixtures prepared by mix-H and the simulation patterns. The simulation was performed by summing up 50% lower-energy shifted (0–0.30 eV, 0.01-eV step) ERDT pattern of PC-101 (anatase) and 50% measured ERDT pattern of isolated-anatase (ANA) / isolated-rutile (RUT), the ζ_s with the measurement ERDT pattern of mix-H was calculated and selected the highest one as the simulation result (for details, see 2.3.2). It can be seen from Fig. 3-13 that the ΔE_{\max} of mix-H of PC-101 (anatase) and isolated-anatase (ANA) is 0.12 eV with a 0.85 ζ_s , ΔE_{\max} of mix-H of PC-101 (anatase) and isolated-rutile (RUT) is 0.17 eV with a 0.80 ζ_s . This may suggest that the h-DOS(VB) of isolated-anatase (ANA) is 0.12 eV higher than that of PC-101 (anatase), at the same time the h-DOS(VB) of isolated-rutile (RUT) is 0.17 eV higher than that of PC-101 (anatase). These are consistent with the previous result that the h-DOS(VB) of rutile isolated from P25 is 0.05 eV higher than that of anatase isolated from P25.

Therefore, the band structure of anatase and rutile isolated from p25 can be evaluated by ERDT analyses. As shown in Fig. 3-14, the h-DOS(VB) of isolated-rutile (RUT) is same with commercial rutile (CR-EL) and about 0.05 eV higher than that of anatase isolated from P25, about 0.17 eV higher than that of commercial anatase (PC-101). The h-DOS(VB) of isolated-rutile (RUT) is same with commercial rutile (CR-EL) and about 0.05 eV higher than that of anatase isolated from P25, about 0.17 eV higher than that of commercial anatase (PC-101).

The anatase isolated from P25 shows an interesting h-DOS(VB) position that is different with the other commercial anatase like PC-101. It can be seen from Figure. 3-13 that the ERDT pattern of isolated-anatase (ANA) seems shifts to the low energy side compared to other anatase samples (the peak of ERDT pattern of isolated-anatase (ANA) in energy located around 3.05 eV, that of other anatase samples was in energy located around 3.2 eV). A possible reason for ΔE_{\max} values of isolated-anatase (ANA) was different with the other anatase samples might be the surface of isolated-anatase (ANA) is tightly attached with some fine rutile layer, and these rutile layer make the ERDT pattern of isolated-anatase (ANA) seems shifts to the low energy side compared to other anatase samples. Considering the above result that the isolated-anatase (ANA) and isolated-rutile (RUT) can be seen as the anatase and rutile composition of HomoP25, the surface of anatase composition of HomoP25 may tightly attached with some fine rutile layer, this may be an interesting finding for researchers studying P25.

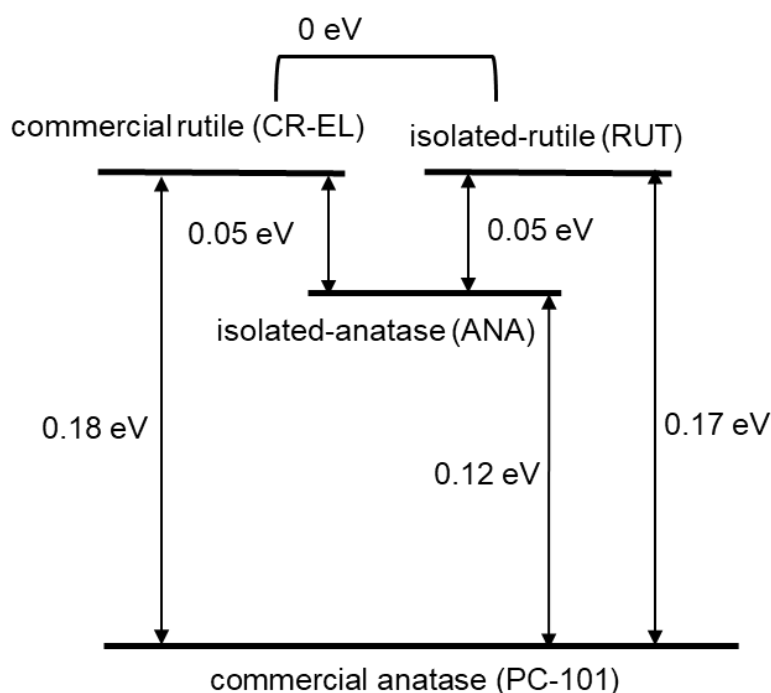


Fig. 3-14 Estimation of band structure of commercial titania samples and anatase, rutile isolated from p25 through energy-resolved distribution of electron traps.

3.3.5 Evaluation of the Relative Band Structure for Various Metal-oxides

Earlier in this chapter I focused on evaluation of the relative band structure of titania samples through energy-resolved distribution of electron traps analysis. As shown in Fig. 3-15, similar analysis was performed with titania and other metal oxides, for example cerium(IV) oxide (CeO_2) and tungsten(VI) oxide (WO_3). Simulated patterns were prepared by summing up 50% lower-energy shifted (0–0.30 eV, 0.01-eV step) ERDT pattern of CeO_2 or WO_3 with 50% measured ERDT pattern of CR-EL (rutile), the ζ_s with the measurement ERDT pattern of mix-0 and mix-H was calculated and selected the highest one as the simulation result. In both cases, ΔE_{max} for ERDT patterns of 50/50 mixture prepared by mix-0 was negligible with almost no energy shift each other, as seen for the mix-0 with titania samples. These results support the hypothesis described in chapter 2 that there was almost no electronic contact between original particles in mix-0 and electron excitation from each VB to each ETs occurred independently. In the case of mix-H, simulation pattern shifted to lower energy side showed better similarity with

ERDT pattern of mix-H. This suggests that interparticle charge-transfer excitation from h-DOS(VB) of a higher-h-DOS(VB) sample to all ETs occurs in the mix-H other than mix-H of titania. In addition, this also means that the energy shifts showing highest ζ_s reflect the actual difference of h-DOS(VB)s between the original samples, when assuming they are mixed thoroughly. Fig. 3-15 shows that the ΔE_{\max} of mix-H of CeO₂ and CR-EL (rutile) is 0.12 eV with a 0.71 ζ_s , ΔE_{\max} of mix-H of WO₃ and CR-EL (rutile) is 0.14 eV with a 0.80 ζ_s . This may suggest that the h-DOS(VB) of CR-EL (rutile) is 0.12 eV higher than that of CeO₂ and 0.14 eV higher than that of WO₃.

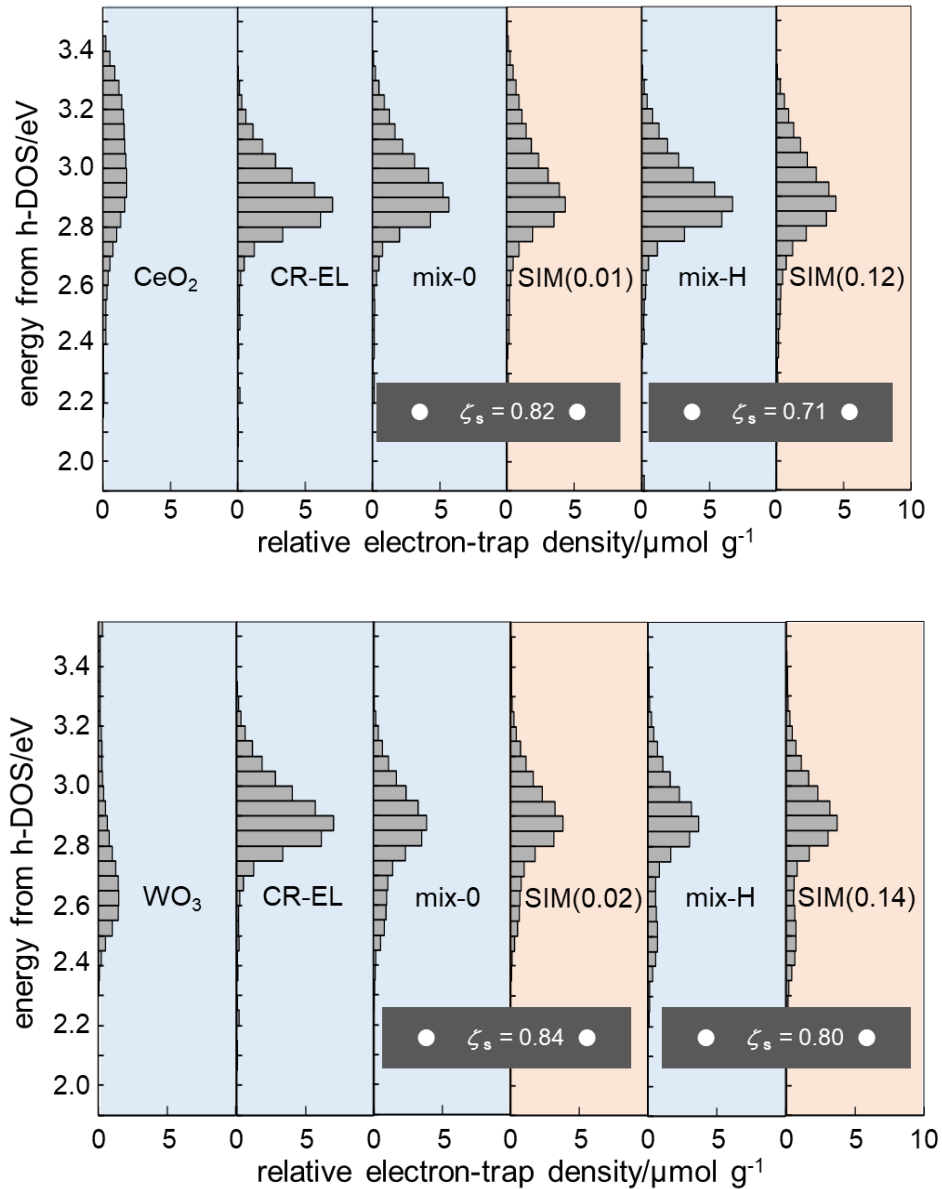


Fig. 3-15 ERDT patterns of CeO₂, WO₃, CR-EL(rutile), and their 50/50 mixtures prepared by different mixing procedures as well as two simulation patterns with different energy shift showing the highest ζ_s with ERDT patterns of mix-0 and mix-H. Blue and orange colors in background indicate experimental and simulation pattern, respectively.

3.4 Conclusions

In this chapter, ΔE_{\max} values of different kinds of titania mixtures were examined and found that the ΔE_{\max} values for most mixtures with rutile and anatase prepared by mix-H were 0.18–0.19 eV. The ΔE_{\max} obtained from the ERDT pattern with homogeneously mixing samples was constant with change in the anatase content, suggesting that the constant ΔE_{\max} reflects the energy difference between h-DOS (VB)s of anatase and rutile in mixture samples. This suggests that the h-DOS(VB) of most anatase were lower than that of most rutile by ca. 0.20 eV and that photoexcitation from h-DOS(VB) of rutile samples to ETs of anatase samples might occur in the mixture samples. Meanwhile, the ionization energy of samples was estimated from photoelectron yield spectroscopy and has been regarded as VBT position and the bandgap can be estimated by PAS spectra. Thus, these results can be used to estimate the relative band structure of metal-oxide samples.

Anatase particles and rutile particles isolated from P25 sample by chemical dissolution method were characterized by RDB-PAS to elucidate their actual position of valence-band. The h-DOS(VB) of isolated-rutile (RUT) is the same as that of commercial rutile. However, the anatase isolated from P25 shows an interesting h-DOS(VB) position that is ca. 0.12 eV higher than most commercial titania sample, this might be due to the surface of anatase composition of HomoP25 may tightly attached with some fine rutile layer resulting in the ERDT pattern of isolated-anatase (ANA) seems shifts to the low energy side compared to other anatase samples.

ΔE_{\max} values of different kinds of metal-oxide mixtures were also examined and estimated their relative band structure through energy-resolved distribution of electron traps analysis. Thus, RDB-PAS analysis of ERDT patterns of mixtures of different titania samples is a novel method to clarify the relative band position of semiconducting metal oxides such as titania.

3.5 References

- Fujishima 2000** Fujishima A, Rao T N, Tryk D A. Titanium dioxide photocatalysis[J]. *Journal of photochemistry and photobiology C: Photochemistry reviews*, **2000**, 1(1): 1-21.
- Hoffmann 1995** Hoffmann M R, Martin S T, Choi W, et al. Environmental applications of semiconductor photocatalysis[J]. *Chemical reviews*, **1995**, 95(1): 69-96.

Shiraishi 2008 Shiraishi Y, Hirai T. Selective organic transformations on titanium oxide-based photocatalysts[J]. *Journal of Photochemistry and Photobiology C: Photochemistry Reviews*, **2008**, 9(4): 157-170.

Tang 1993 Tang H, Berger H, Schmid P E, et al. Photoluminescence in TiO₂ anatase single crystals[J]. *Solid State Communications*, **1993**, 87(9): 847-850.

Minoura 1985 Minoura H, Nasu M, Takahashi Y. Comparative studies of photoelectrochemical behaviours of rutile and anatase electrodes prepared by OMCVD technique[J]. *Berichte der Bunsengesellschaft für physikalische Chemie*, **1985**, 89(10): 1064-1069.

Scanlon 2013 Scanlon D O, Dunnill C W, Buckeridge J, et al. Band alignment of rutile and anatase TiO₂ [J]. *Nature materials*, **2013**, 12(9): 798-801.

Zhang 2014 Zhang J, Zhou P, Liu J, et al. New understanding of the difference of photocatalytic activity among anatase, rutile and brookite TiO₂[J]. *Physical Chemistry Chemical Physics*, **2014**, 16(38): 20382-20386.

Nitta 2016 Nitta A, Takase M, Takashima M, et al. A fingerprint of metal-oxide powders: energy-resolved distribution of electron traps[J]. *Chemical Communications*, **2016**, 52(81): 12096-12099.

Nitta 2019 Nitta A, Takashima M, Takase M, et al. Identification and characterization of titania photocatalyst powders using their energy-resolved distribution of electron traps as a fingerprint[J]. *Catalysis Today*, **2019**, 321: 2-8.

Nitta 2018 Nitta A, Takashima M, Murakami N, et al. Reversed double-beam photoacoustic spectroscopy of metal-oxide powders for estimation of their energy-resolved distribution of electron traps and electronic-band structure[J]. *Electrochimica acta*, **2018**, 264: 83-90.

Buchalska 2015 Buchalska M, Kobielusz M, Matuszek A, et al. On oxygen activation at rutile-and anatase-TiO₂[J]. *ACS Catalysis*, **2015**, 5(12): 7424-7431.

Shen 2020 Shen Y, Nitta A, Takashima M, et al. Do Particles Interact Electronically?—Proof of Interparticle Charge-Transfer Excitation between Adjoined Anatase and Rutile Particles[J]. *Chemistry Letters*, **2020**, 49(X).

Amano 2009

Amano 2009 Amano F, Yasumoto T, Prieto-Mahaney O O, et al. Photocatalytic activity of octahedral single-crystalline mesoparticles of anatase titanium (IV) oxide[J]. *Chemical communications*, **2009** (17): 2311-2313.

Wang 2018 Wang K, Wei Z, Ohtani B, et al. Interparticle electron transfer in methanol dehydrogenation on platinum-loaded titania particles prepared from P25[J]. *Catalysis Today*, **2018**, 303: 327-333.

Toyoda 2015 Toyoda T, Yindeesuk W, Okuno T, et al. Electronic structures of two types of TiO₂ electrodes: inverse opal and nanoparticulate cases[J]. *RSC Advances*, **2015**, 5(61): 49623-49632.

Ikeda 2003 Ikeda S, Sugiyama N, Murakami S, et al. Quantitative analysis of defective sites in titanium (IV) oxide photocatalyst powders[J]. *Physical Chemistry Chemical Physics*, **2003**, 5(4): 778-783.

Quantitative Measurement of the Hetero-contact Degree of Metal-oxide Mixtures

4.1 Introduction

The design and development of hetero-structured photocatalysts is a promising strategy to improve photocatalytic activity. Many researchers have claimed that the reason for the improvement in photocatalytic performance of hetero-structured photocatalyst is that the electron-hole recombination is reduced by the charge transfer between original particles [Bickley 1991/ Kamat 1993/ Hurum 2003/ Ohno 2003/Sun 2018]. In other words, homogeneously mixing and sufficient contact between nanoparticles is important. However, in previous studies, the concept of hetero-contact degree was either defined by mathematical simulation [Siiriä 2009/ Yeoh 2005/ Kim 2007] or estimated based on calculating the probability distribution of local averages of the desired property (such as mass, density or color) [Cleary 1998/ Suetsugu 1990/ Bur 2004], there is no method to quantitatively evaluation the contact condition between nanoparticles. In this study, ERDT analysis provides quantitative measurement of the hetero-contact degree, which is a new concept and has not been measured so far.

In Chapter 2, I discussed interparticle charge-transfer excitation (ICTE), that is photoexcitation from the h-DOS(VB) of the higher h-DOS(VB) sample (rutile) to all ETs at an anatase-rutile interface. This electronic interaction requires close contact between original particles in the mixture. ICTE analysis suggested a new concept, hetero-contact degree, which could be quantitatively evaluated by comparison of ERDT patterns of mixture sample to simulation patterns with thoroughly adjoined mixture particles and non-contacted particles. The "hetero-contact degree" here means how much proportion of one kind of particles (anatase in the discussion of 4.3.1) are electronically contacted with the other kind of particles (in the discussion of 4.3.1). In this chapter, ERDT analysis to provides quantitative measurement of the hetero-contact degree was further studied.

4.2 Experimental

4.2.1 Materials

Commercial metal oxide samples, laboratory-made octahedral shape anatase (OAP) [Amano 2009] and samples from Japan Reference Catalyst (JRC-TIO series) supplied by

the Catalysis Society of Japan (CSJ) was used in this study, their properties are shown in Table 3-1. The details of mix-0, mix-L and mix-H are described in 2.2.1.

4.2.2 Photoacoustic Spectroscopy (PAS) and Reversed Double-beam Photoacoustic Spectroscopy (RDB-PAS) Measurement

The details are described in 2.2.2.

4.2.3 Scanning Electron Microscope (SEM) Measurement

Scanning electron microscopy (SEM) was used to characterize the morphology of the samples by using JEOL JSM-7400F instruments.

4.2.4 X-ray Diffraction (XRD) Measurement

XRD analysis was performed using the X-ray diffractometer with the data acquisition conditions as follows: 2θ range, $10\text{--}90^\circ$; scan speed, $10^\circ\cdot\text{min}^{-1}$; and scan step, 0.008° . Crystallinity of the sample was estimated using highly crystalline nickel oxide as an internal standard. The standard (20 wt %) was mixed thoroughly with a sample (80 wt %) by braying in an agate mortar.

4.2.5 Brunner–Emmet–Teller (BET) Measurement

Specific surface area estimated by Brunauer-Emmett-Teller (BET) equation from nitrogen adsorption amount measured with Quantachrome Autosorb-6 at 77 K.

4.2.6 Gas Phase Reaction Performance Measurement

Gas phase reaction performance of samples were tested under UV irradiation for oxidative decomposition of acetaldehyde. Sample were set in PAS sample holder in the reactor (cylindrical glass reactor). First of all, samples were irradiated by a UV LED light to remove adsorbed impurities. When the carbon dioxide content in the reactor is stable, fill the reactor with 0.2ml gaseous acetaldehyde, then put the reactor in a dark environment until the gaseous acetaldehyde content in the reactor is stable. For reaction performance measurement, samples were irradiated by a UV LED light (HMP-5).

Reactions were monitored by measurement acetaldehyde residue and liberation of CO₂ by gas chromatography.

4.3 Results and Discussion

4.3.1 Quantitative Analysis of Hetero-contact Degree of Mixture Samples of Anatase and Rutile

The hetero-contact degree of mixture samples of anatase and rutile prepared by different mixing procedures was briefly discussed in 2.3.3, and found that the interesting ERDT pattern of mix-L which seems to be spliced by two ERDT patterns might be due to the presence of two kinds of anatase particles, with and without electronic contact with rutile particles, in 35% and 65% composition. In this part I will discuss this calculation process in detail.

As shown in Fig. 4-1, in order to reproduce the interesting ERDT pattern of mix-L which prepared by mixed ST-21 and ST-G1 with a Teflon spatula gently for 20 min (see Fig. 2-5), simulated ERDT patterns was performed by summation of the $(100 - X)\%$ ERDT pattern of SIM(0) which represents a 0% hetero-contact degree and $X\%$ ($X = 0 - 100$, 5 step) ERDT pattern of SIM(0.19) which represents a 100% hetero-contact degree.

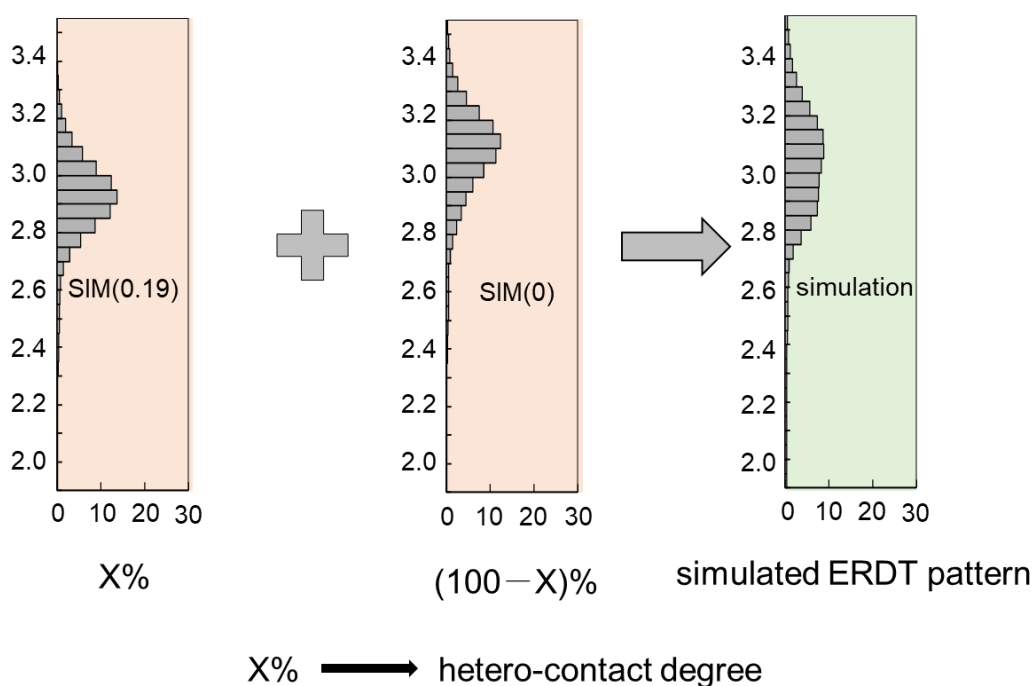


Fig. 4-1 Simulated ERDT patterns of 50/50 mixture for anatase ST-21 and rutile ST-G1 prepared by mix-L.

The ERDT patterns of ST-21, ST-G1, their 50/50 mixture prepared by mix-L, and simulation patterns with hetero-contact degree from 0–100% are shown in Fig. 4-2. Green and blue colors in the background indicate simulation and as-measured patterns, respectively. It can be seen that with increase in the hetero-contact degree ($X\%$), the peak of simulated ERDT pattern shifted lower energy side and some simulated ERDT pattern shown two peaks (30%, 35%, 40%). Calculations of ζ_s with these simulated ERDT patterns and as-measured ERDT pattern of mix-L are shown in Fig. 4-3, the hetero-contact degree giving the highest ζ_s was selected as $X\%_{\max}$, the corresponding simulation result is also regarded as suitable simulation result for mix-L. For the 50/50 mixture of ST-21 and ST-G1, it can be seen that with increase in the hetero-contact degree ($X\%$), ζ_s also increased up to 0.80 (a relatively high value) at the hetero-contact degree of 35%, then decreased with increase in the hetero-contact degree ($X\%$), this means that the measured ERDT pattern of mix-L could be reproduced by assuming there are two kinds of anatase particles in mix-L, with and without electronic contact with rutile particles, in 35% and 65% composition.

35% anatase particles were electronic contact with rutile particles, their ERDT shifted to lower energy side can be reproduced by SIM(0.19). At the same time, 65% anatase particles without electronic contact with rutile particles, their ERDT remain unchanged can be reproduced by SIM(0). In other words, the ERDT analysis suggested a new concept, hetero-contact degree, which could be quantitatively evaluated by comparison of ERDT patterns of mixture sample to simulation patterns with thoroughly adjoined mixture particles and non-contacted particles. The "hetero-contact degree" here means how much proportion of one kind of particles (anatase in this discussion) are electronically contacted with the other kind of particles (rutile in this discussion).

Hetero-contact degree is a novel concept that has not been measured so far, because such quantitative measurement requires macroscopic analysis collecting the information on particle contact. As shown in Fig. 4-4 and Fig. 4-5, the bulk composition and specific surface area of ST-21, ST-G1, their 50/50 mixture prepared by mix-0, mix-L and mix-H were almost same and can be reproduced by simple summation of ST-21 and ST-G1 (the average of bulk composition and specific surface area ST-21 and ST-G1). Therefore, XRD and BET are the representative macroscopic powder analyses, but they have no information on anatase-rutile particle contact. On the other hand, SEM and TEM might give information on anatase-rutile particle contact, but they are microscopic and no average cannot be obtained. As shown in Fig. 4-6, although the particle sizes of ST-21 and ST-G1 are different, it is difficult to distinguish two different kinds of particles in mix-L and mix-H. It is difficult to use SEM to characterize the hetero-contact degree.

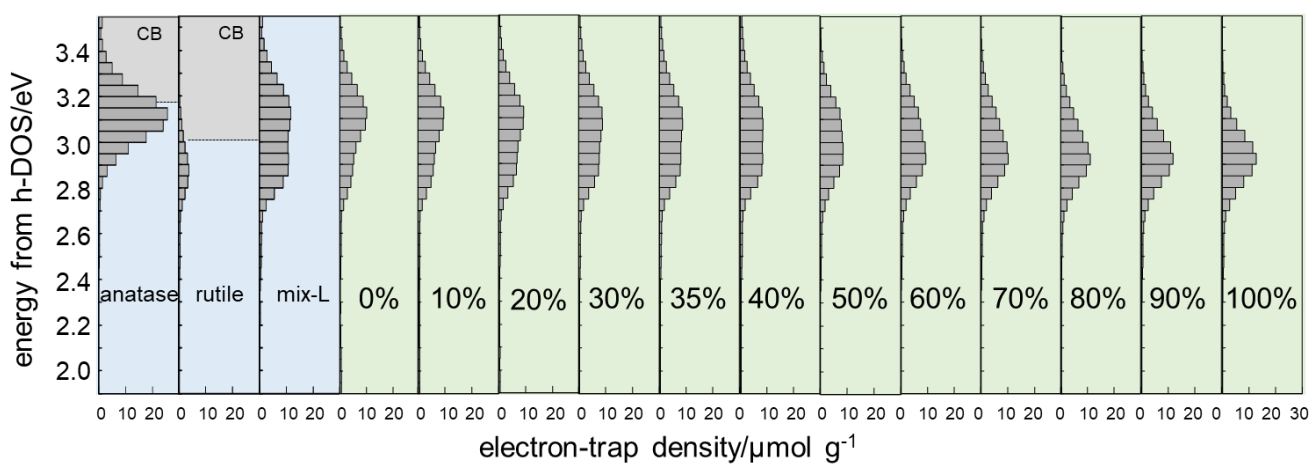


Fig. 4-2 ERDT patterns of ST-21, ST-G1, and 50/50 mixture prepared by mix-L, and simulation patterns with hetero-contact degree from 0–100%. Green and blue colors in the background indicate simulation and as-measured patterns, respectively.

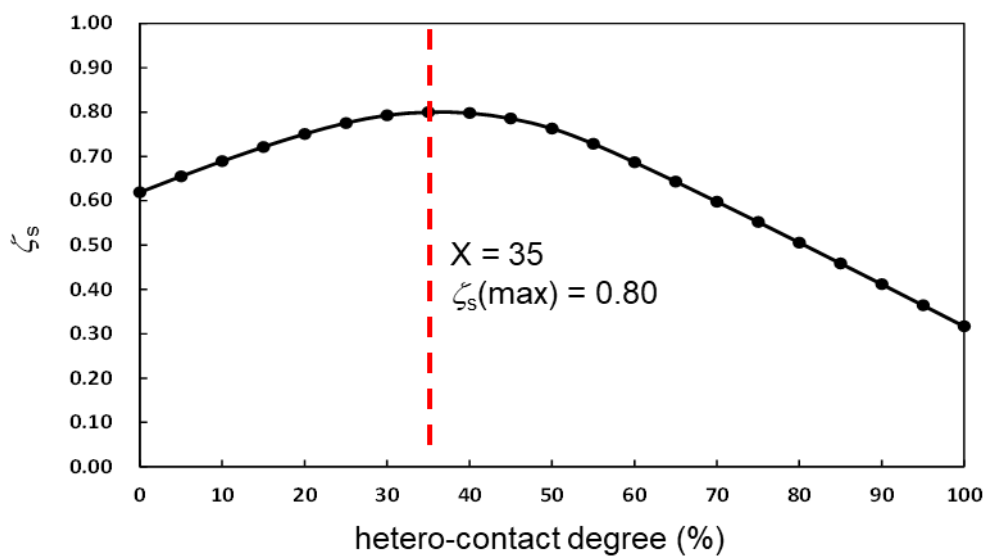


Fig. 4-3 Hetero-contact degree and degree of coincidence of the ERDT patterns (ζ_s) for ST-21 and ST-G1 50/50 mixtures prepared by mix-L.

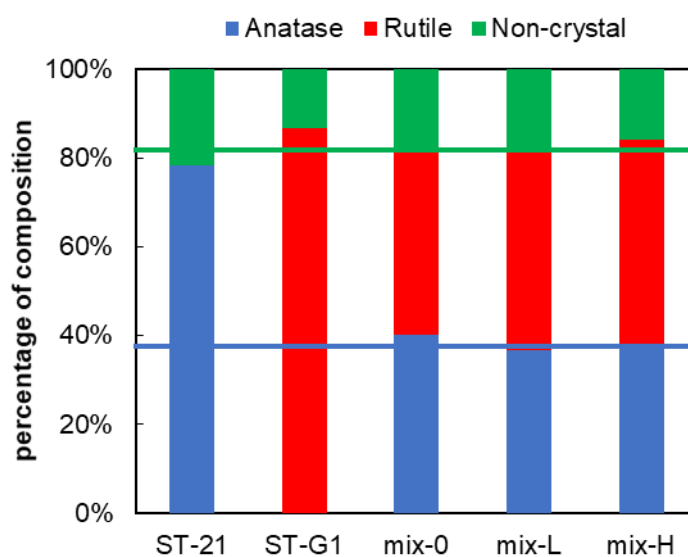


Fig. 4-4 Bulk composition of ST-21, ST-G1, their 50/50 mixture prepared by mix-0, mix-L and mix-H, and the average of bulk composition ST-21 and ST-G1. The non-crystalline was obtained from Rietveld analysis measured by a Rigaku Smart Lab X-ray diffractometer with 20wt% nickel (II) oxide. Mix-0 means that ST-21 and ST-G1 were half to half separately loaded on the sample holder (no mixing) during the measurement. The green and blue lines represent the average values of amorphous phase and anatase phase, respectively.

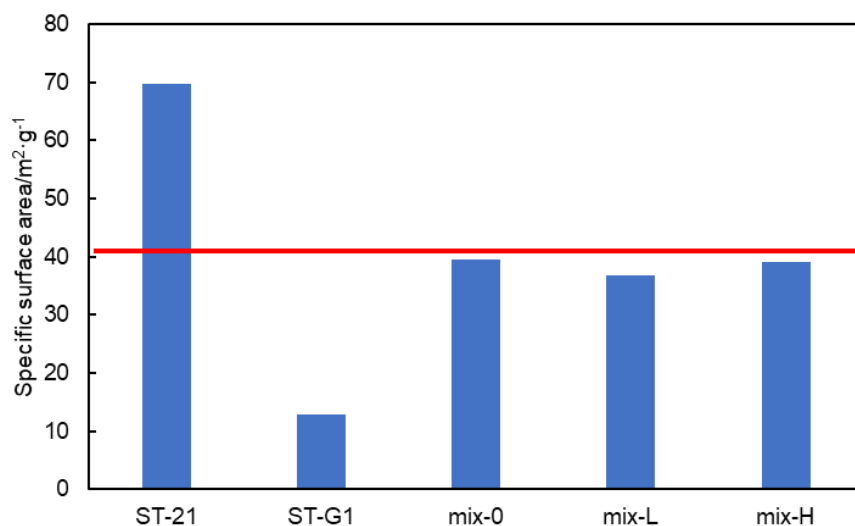


Fig. 4-5 Specific surface area of ST-21, ST-G1, their 50/50 mixture prepared by mix-0, mix-L and mix-H, and the average of bulk composition ST-21 and ST-G1. Mix-0 means that ST-21 and ST-G1 were just put into the BET cell in equal amounts during the measurement without mixing. The red line represents the average specific surface area value of anatase and rutile.

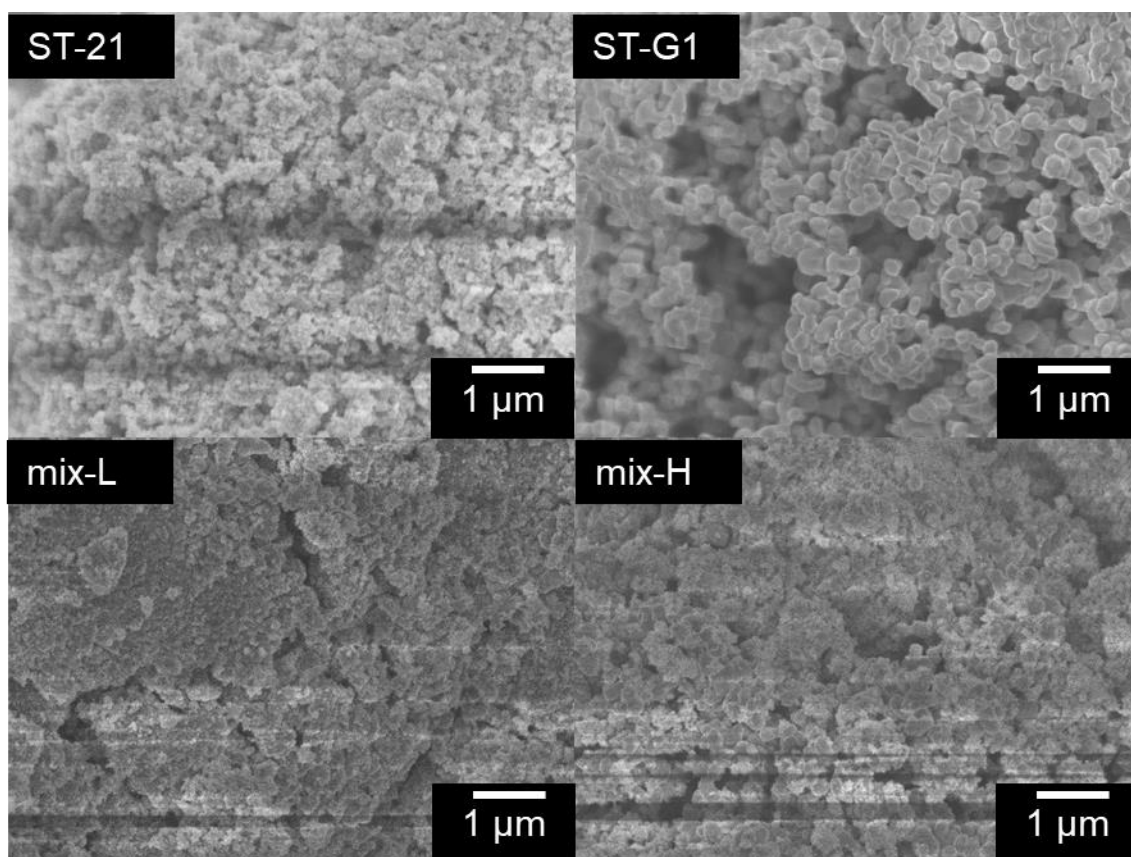


Fig. 4-6 SEM pictures of ST-21, ST-G1, the mix-L and the mix-H.

4.3.2 *Hetero-contact Degree of Mixture Samples of Anatase and Rutile Prepared by Different Mixing Time*

For further research, the ERDT patterns of mix-L prepared by different mixing time of octahedral shape anatase particle (OAP) and HT-0514 were examined as shown in Fig. 4-7. The simulation ERDT patterns of Fig. 4-7 is simulated in the manner described in 2.3.2, that is, it is assumed that the mixtures were homogeneously mixing with thoroughly adjoined mixture particles. In other words, the hetero-contact degree of mixture is 100%. It can be seen from Fig. 4-7 that the ΔE_{\max} of mix-L-5 was 0.02 eV with a 0.75 ζ_s , mix-L-10 was 0.15 eV with a 0.80 ζ_s , mix-L-15 was 0.17 eV with a 0.84 ζ_s , as the mixing time increase, ΔE_{\max} and ζ_s also increase. In addition, the ERDT patterns of mix-L prepared by different mixing time seems different. Especially for mix-L-5, there are significantly more ETs located in the high energy range (3.1 eV-3.25 eV) of mix-L-5 than that of the other two, and the ζ_s of mix-L-5 is relatively smaller than the others. This might be due to different mixing time caused different mixing state and original particle contact states. when the mixing time is smaller, original samples' particles were not homogeneously mixed and sufficiently contacted with a lower hetero-contact degree.

Insufficient contact of some OAP particles with HT-0514 particles caused same ETs located in the high energy range (3.1 eV-3.25 eV, inside the red wireframe), and when the simulation was performed by assumed that the mixtures were 100% hetero-contact degree with thoroughly adjoined mixture particles, the ΔE_{\max} (energy shift) and ζ_s (degree of coincidence of the ERDT pattern shape) will become smaller.

In order to get more suitable simulation ERDT patterns, simulated in the manner described in 4.3.1, that is, it is assumed that the mixtures were inhomogeneous mixing with insufficient contact mixture particles. In other words, the hetero-contact degree of mixtures is lower than 100%. As shown in Fig. 4-8, the hetero-contact degree of mix-L-5 was 35% with a 0.88 ζ_s , mix-L-10 was 65% with a 0.92 ζ_s , mix-L-15 was 80% with a 0.90 ζ_s . Degree of coincidence of the ERDT pattern shape of simulated assumed that the hetero-contact degree of mixtures is lower than 100% with as-measured was higher than that of simulated assumed that the mixtures have a 100% hetero-contact degree. Obviously, the simulated ERDT patterns with assumed the hetero-contact degree of mixtures are lower than 100% were more suitable than that of with assumed the mixtures have a 100% hetero-contact degree. Especially for the high energy range (3.1 eV-3.25 eV, inside the red wireframe).

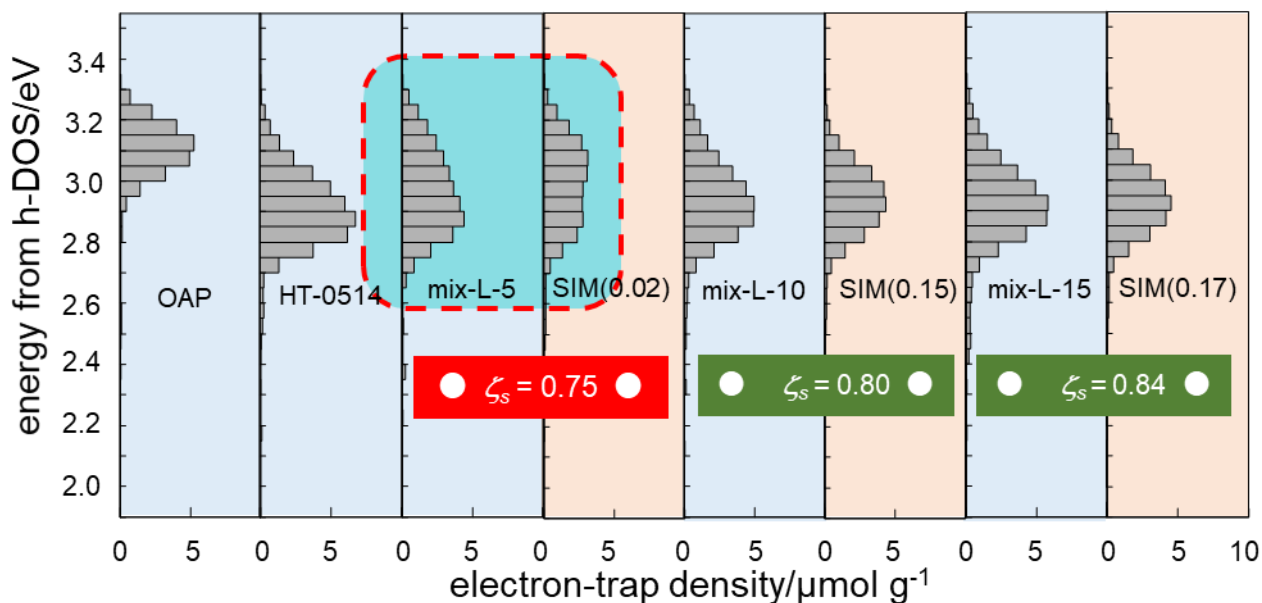


Fig. 4-7 ERDT patterns of OAP, HT-0514, their 50/50 mixture prepared by mix-L with 5min, 10min, 15min, and simulation patterns with 100% hetero-contact degree hypothesis. Orange and blue colors in the background indicate simulation and as-measured patterns, respectively.

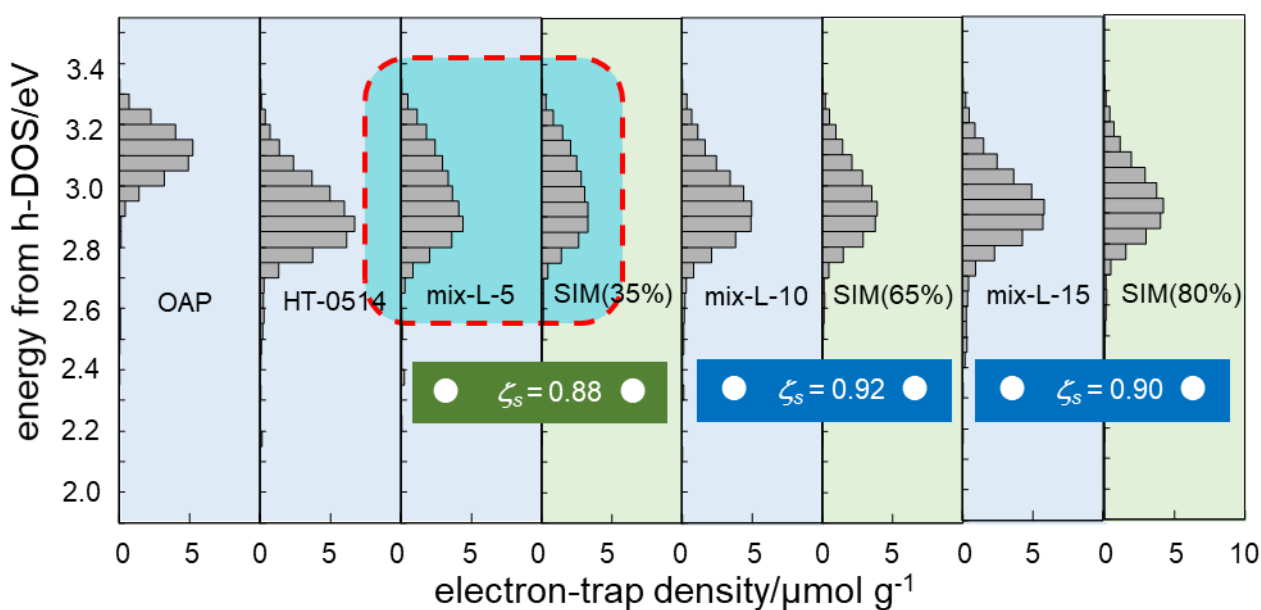


Fig. 4-8 ERDT patterns of OAP, HT-0514, their 50/50 mixture prepared by mix-L with 5min, 10min, 15min, and simulation patterns with lower than 100% hetero-contact degree hypothesis. Green and blue colors in the background indicate simulation and as-measured patterns, respectively.

It is easily to expect that as the mixing time increase, the hetero-contact degree of the mixture will be improved, but traditional analysis methods cannot obtain a quantitative hetero-contact degree. Since it is difficult to distinguish two different kinds of particles in mixture of ST-21 and ST-G1 in 4.3.1, octahedral shape anatase particles (OAPs) with a special particle morphology were used in this part. As shown in Fig. 4-9, benefit from the regular appearance of OAPs, it is easily to distinguish OAP from HT-0514 and we can clearly see the contact between OAP particles and HT-0514 particles. However, the SEM pictures give us some information on particle contact, but they are microscopic and cannot give a quantified value of hetero-contact degree like ERDT

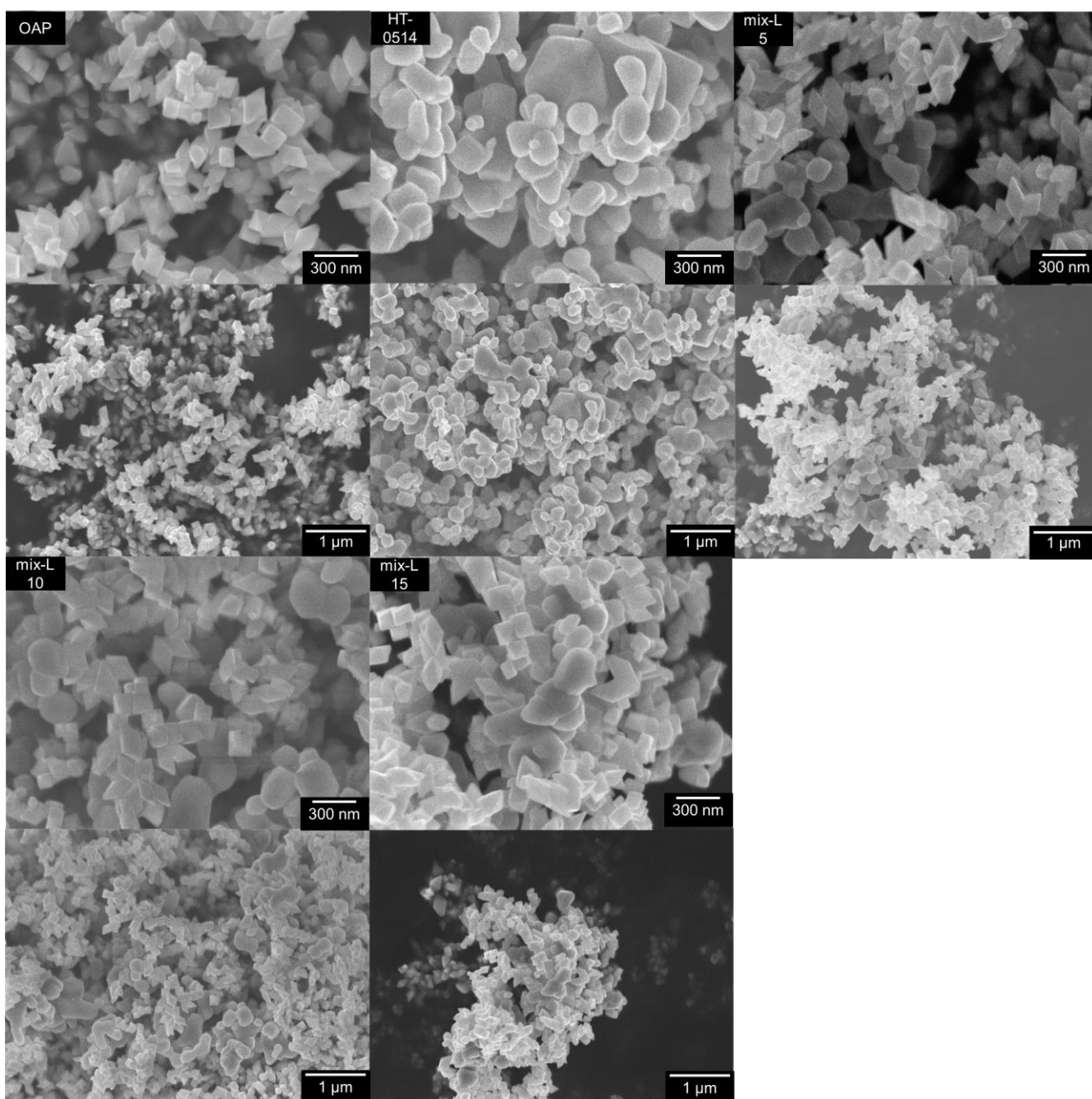


Fig. 4-9 SEM pictures of OAP, HT-0514, and their mixtures prepared by mix-L with different mixing time.

analysis.

4.3.3 Hetero-contact Degree of Mixture Samples of Anatase and Rutile Prepared by

Different Anatase Contents

The ERDT patterns of mix-H prepared by different anatase (OAP) content of octahedral shape anatase particle (OAP) and ST-G1 were examined as shown in Fig. 4-10. The simulation ERDT patterns of Fig. 4-10 is simulated in the manner described in 2.3.2, that is, it is assumed that the mixtures were homogeneously mixing with thoroughly adjoined mixture particles. In other words, the hetero-contact degree of mixture is 100%. It can be seen from Fig. 4-10 that the ΔE_{\max} of mix-H-0.3 was 0.18 eV with a 0.82 ζ_s , mix-H-0.4 was 0.20 eV with a 0.79 ζ_s , mix-H-0.5 was 0.18 eV with a 0.80 ζ_s , mix-H-0.6 was 0.17 eV with a 0.74 ζ_s , mix-H-0.7 was 0.17 eV with a 0.80 ζ_s , mix-H-0.9 was 0.14 eV with a 0.66 ζ_s , mix-H-0.95 was 0.13 eV with a 0.69 ζ_s . As shown in Fig. 4-11, when anatase (OAP) content was 0.3-0.7, the ΔE_{\max} and ζ_s remain stable (ca. 0.19 eV and ca. 0.80). On the other hand, the ΔE_{\max} and ζ_s of mix-H with anatase (OAP) content was 0.9 and 0.95 were relatively low compared to others. As discussed in 3.3.2 that with lower anatase content, almost all of the anatase (OAP) particles were in sufficient contact with rutile (ST-G1) particles, while at a higher anatase content, not all of the anatase (ST-21) particles had sufficient contact with rutile (ST-G1) particles, this caused same ETs located in the high energy range (3.1 eV-3.25 eV, inside the red wireframe) of mixture will resulting in the decrease in observed ΔE_{\max} and ζ_s when the simulation was performed by assumed that the hetero-contact degree of mixtures are 100%. Such qualitative analysis conclusions can be easily obtained, but there is no traditional analysis method to help us quantitatively measure the degree of hetero-contact status (here means how much proportion of OAP particles were electronically contacted with the ST-G1 particles).

In order to get more suitable simulation ERDT patterns and quantitatively measure the hetero-contact degree, simulated in the manner described in 4.3.1, that is, it is assumed that the hetero-contact degree of mixtures is lower than 100%. As shown in Fig. 4-12, the hetero-contact degree of mix-H-0.3 was 85% with a 0.89 ζ_s , mix-H-0.4 was 90% with a 0.87 ζ_s , mix-H-0.5 was 90% with a 0.87 ζ_s , mix-H-0.6 was 80% with a 0.78 ζ_s , mix-H-0.7 was 85% with a 0.85 ζ_s , mix-H-0.9 was 70% with a 0.85 ζ_s , mix-H-0.95 was 65% with a 0.79 ζ_s . Degree of coincidence of the ERDT pattern shape of simulated assumed that the hetero-contact degree of mixtures is lower than 100% with as-measured were relatively higher than that of simulated assumed that the hetero-contact degree of mixtures is 100%.

Obviously, the simulated ERDT patterns with assumed the hetero-contact degree of mixtures is lower than 100% were more suitable than that of with assumed the hetero-contact degree of mixtures is 100%, especially for the high energy range (3.1 eV-3.25 eV, inside the red wireframe) of mix-H-0.9 and mix-H-0.95.

Consistent with the above qualitative analysis, hetero-contact degree (here means how much proportion of OAP particles were electronically contacted with the ST-G1 particles) of mix-H with anatase (OAP) content was 0.3-0.7 were remain stable and relatively higher (80%-90%) than that of mix-H-0.9 and mix-H-0.95(65%-70%).

As shown in Fig. 4-13, benefit from the regular appearance of OAPs, it is easily to distinguish OAP from ST-G. Similar to 4.3.2, the SEM pictures give some information on particle contact, however, they are microscopic and cannot give a quantified value of hetero-contact degree.

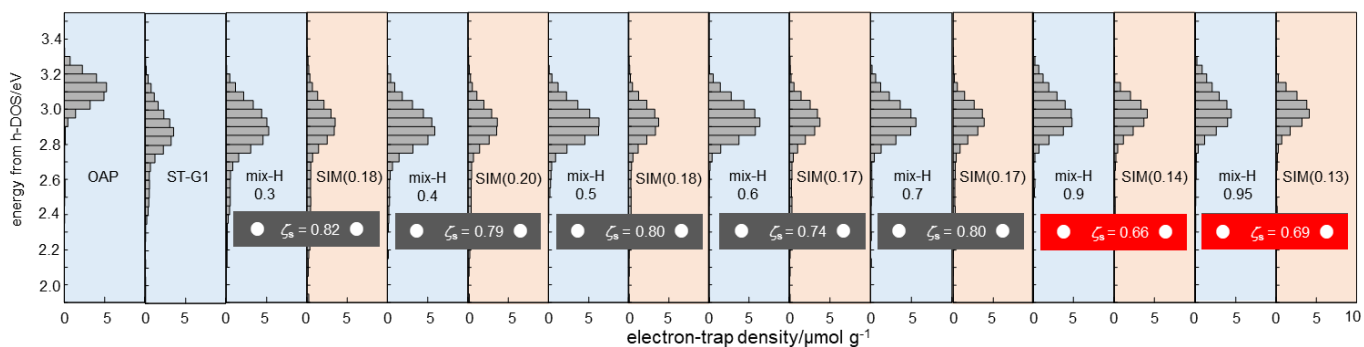


Fig. 4-10 ERDT patterns of OAP, ST-G1, their mix-H prepared by different anatase (OAP) content and simulation patterns with 100% hetero-contact degree hypothesis. Orange and blue colors in the background indicate simulation and as-measured patterns, respectively.

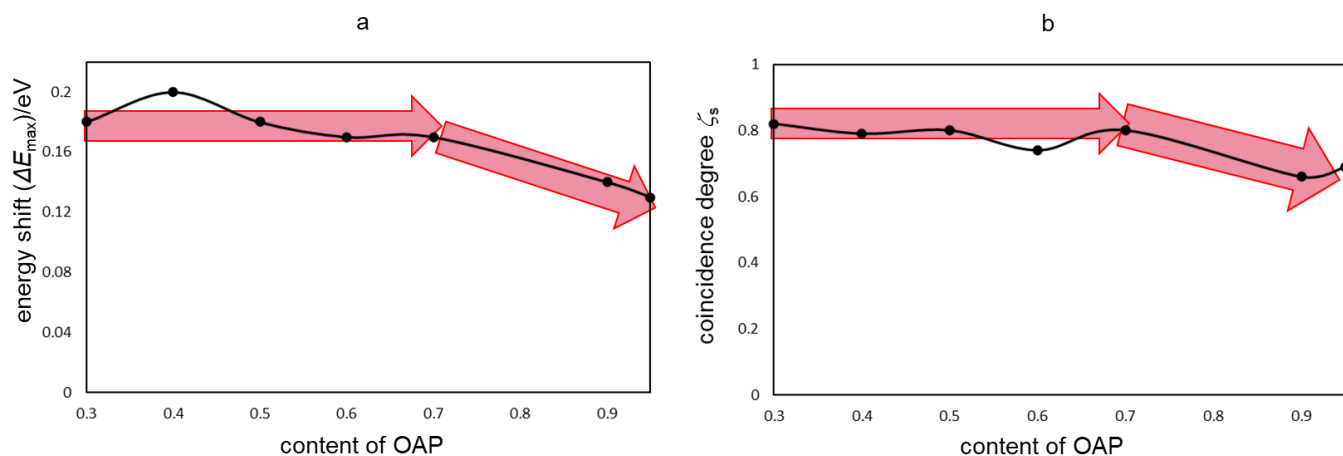


Fig. 4-11 Maximum energy shift (ΔE_{\max}) and ERDT pattern shape coincidence degree (ζ_s) as a function of anatase content in mixtures prepared as mix-H (for simulation patterns with 100% hetero-contact degree hypothesis).

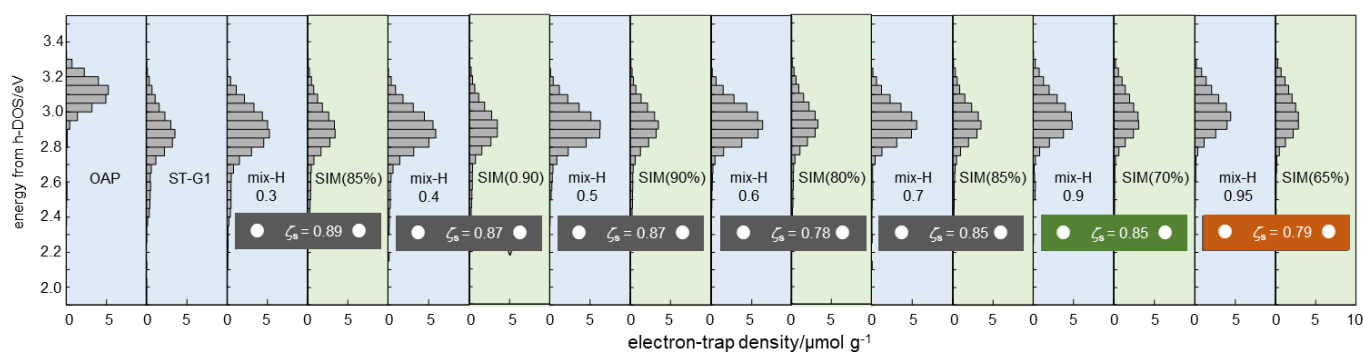


Fig. 4-12 ERDT patterns of OAP, HT-0514, their mix-H prepared by different anatase (OAP) content and simulation patterns with lower than 100% hetero-contact degree hypothesis. Green and blue colors in the background indicate simulation and as-measured patterns, respectively.

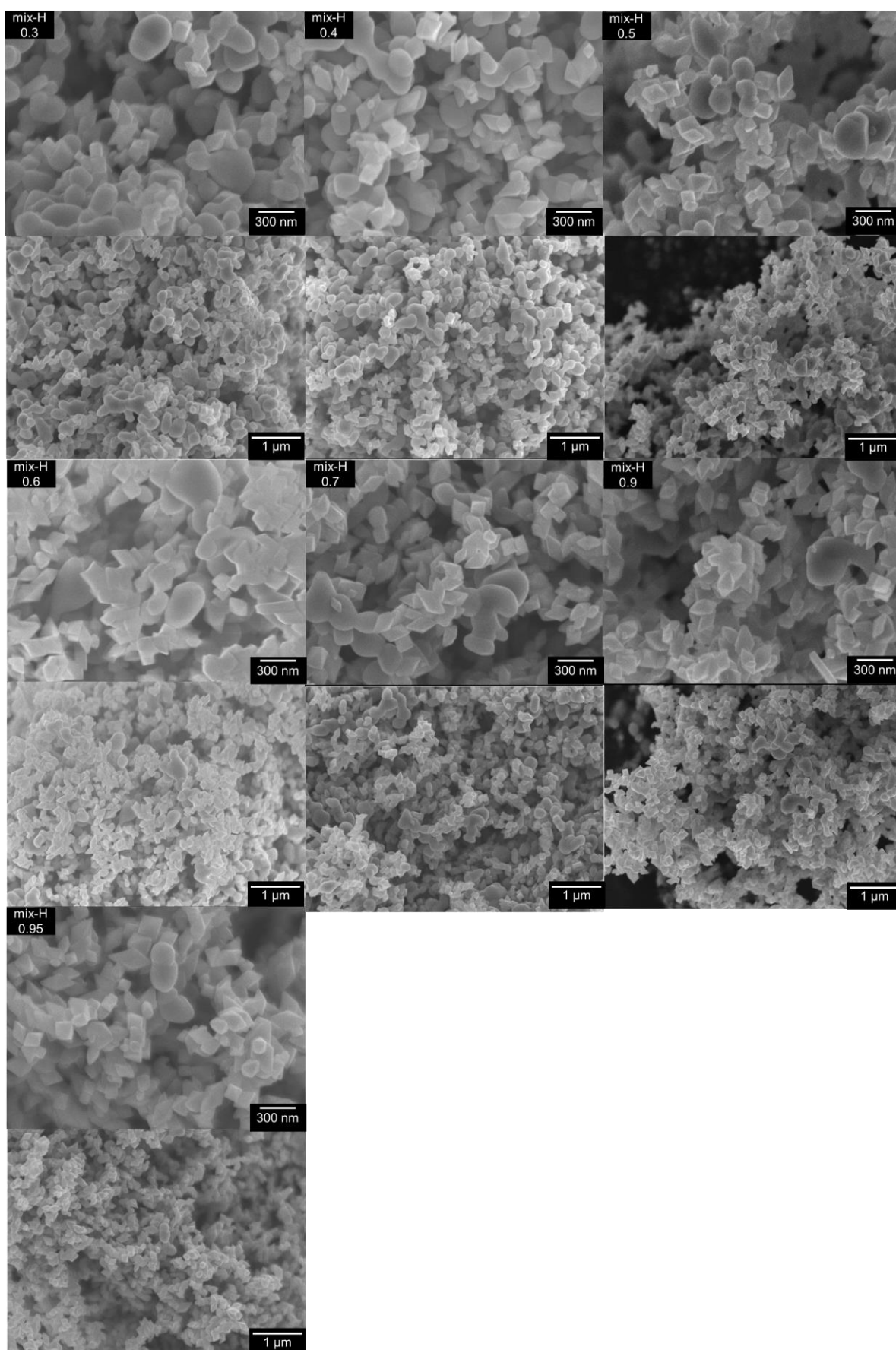


Fig. 4-13 SEM pictures of mix-L prepared by OAP and ST-G1 with different anatase (OAP) content.

4.3.4 Gas Phase Photocatalytic Reaction Performance of Mixtures with Different Hetero-contact degree

In order to study the photocatalytic reaction performance of mixtures with different hetero-contact degree, gas phase reaction of oxidative decomposition of acetaldehyde under UV irradiation were performed as described in 4.2.6 (in the liquid phase reaction, the contact state of the particles in the mixture will change).

The gas phase photocatalytic reaction performance of mix-L of ST-21 and ST-G1 were shown in Fig. 4-14. It can be seen from Fig. 4-14, as the irradiation time increases,

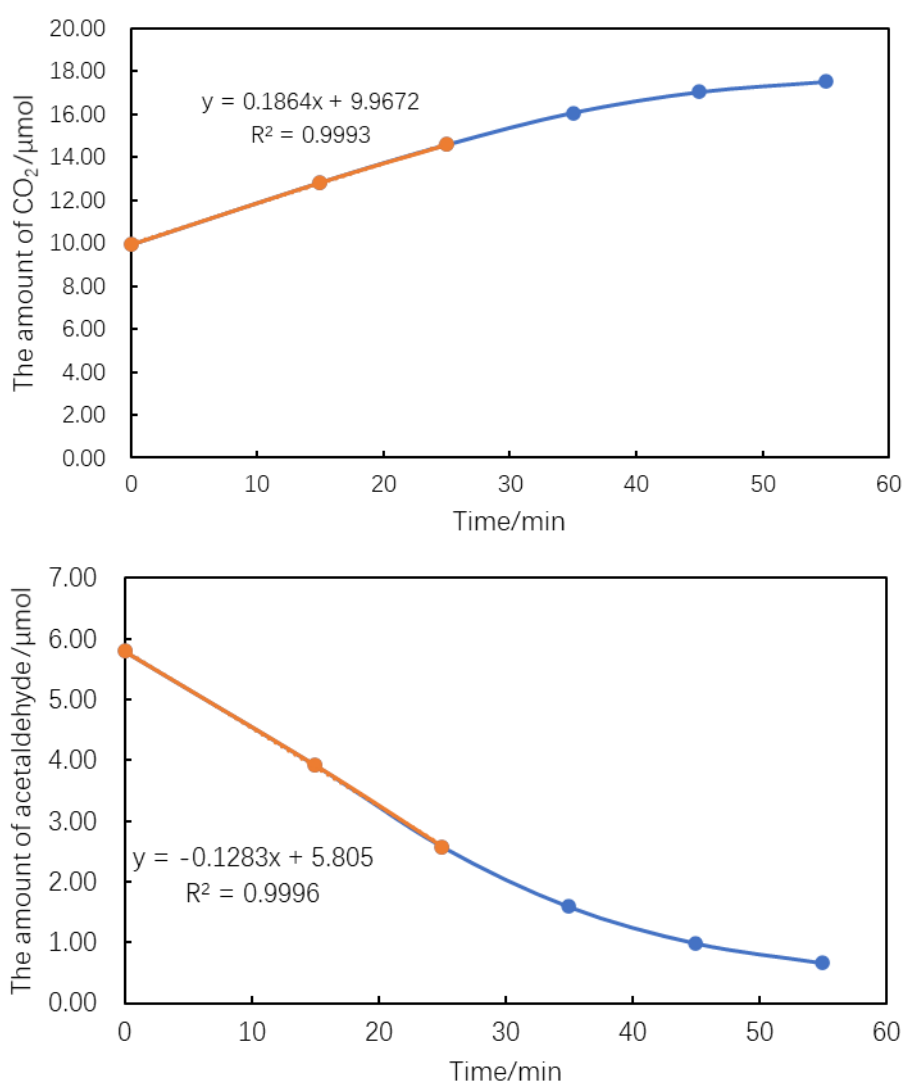


Fig. 4-14 Gas phase reaction performance of mix-L of ST-21 and ST-G1.

the content of carbon dioxide increases and the content of acetaldehyde decreases. This is due to the photocatalytic decomposition of acetaldehyde to produce carbon dioxide. After 25 minutes, the increase rate of carbon dioxide and the decrease rate of acetaldehyde decrease simultaneously because of the decrease of reactant concentration. Based on the data of the first 25 minutes, it is calculated that the decomposition rate of acetaldehyde is $0.13 \mu\text{mol min}^{-1}$, and the generation rate of carbon dioxide is $0.19 \mu\text{mol min}^{-1}$.

The gas phase photocatalytic reaction performance of ST-21, ST-G1, their 50/50 mixture prepared by mix-0, mix-L and mix-H, and the average of reaction rate of ST-21 and ST-G1(AVG) were shown in Fig. 4-15(considering the influence of acetaldehyde adsorption, reactions here were monitored by measurement the liberation of CO_2 by gas chromatography). Mix-0 means that ST-21 and ST-G1 were just half to half separately loaded on the sample holder during the measurement. It can be seen from the picture that the generation rate of carbon dioxide of mix-0 was similar to the average value of reaction rate of ST-21 and ST-G1(about $0.2 \mu\text{mol min}^{-1}$) as expected. On the other hand, mix-L and mix-H showed a little lower activity than that of mix-0. The lowest activity of mix-H which as a sample with the highest hetero-contact degree for carbon-dioxide liberation may suggest that good contact of ST-21 and ST-G1 reduces the reaction efficiency. The possible reason might be in the sample of homogeneously mixing with thoroughly adjoined mixture particles, a considerable part of ST-21 particles is evenly dispersed in the pores of ST-G1 and cannot absorb photons (particle size of ST-21 is smaller than ST-G1). Since ST-21 shown much higher activity than ST-G1, these ST-21 particles, which cannot absorb photons, caused the photocatalytic activity of the mixture to decrease.

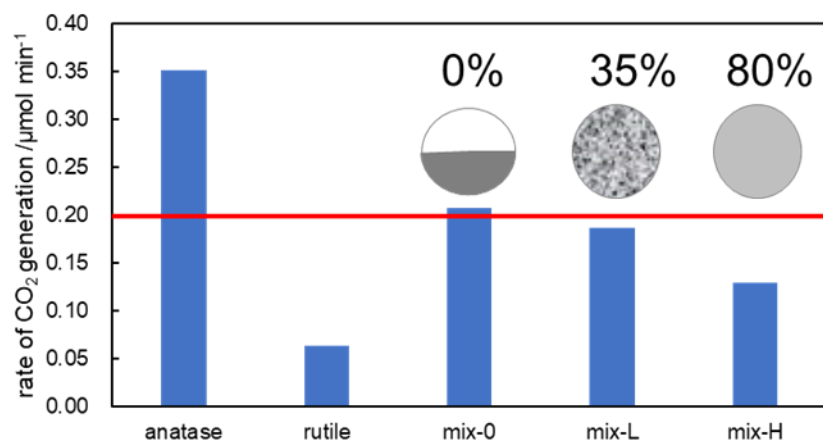


Fig. 4-15 The gas phase photocatalytic reaction performance of ST-21, ST-G1, their 50/50 mixture prepared by mix-0, mix-L and mix-H, and the average of reaction rate of ST-21 and ST-G1. Mix-0 means that ST-21 and ST-G1 were just half to half separately loaded on the sample holder (no mixing) during the measurement. The red line represents the average rate of carbon dioxide generation value of anatase and rutile.

4.4 Conclusions

In this chapter, ERDT analysis provides quantitative measurement of the particle-hetero-contact degree which represents how much proportion of one kind of particles (anatase in this study) are electronically contacted with the other kind of particles (rutile in this study). Mixtures of anatase and rutile prepared by different mixing methods, mixing time and anatase content were characterized to study their particle hetero-contact degree. During the analysis, the simulated ERDT patterns with assumed the hetero-contact degree of mixtures is lower than 100% were more suitable than that of with assumed the hetero-contact degree of mixtures is 100%. Through simple qualitative analysis, it is easy to know that the hetero-contact degree of these mixtures is different. However, only ERDT analysis gives a quantitative value of the particle hetero-contact degree, because such quantitative measurement requires macroscopic analysis collecting the information on particle contact which XRD, BET and SEM cannot give.

The gas phase photocatalytic reaction performance of mixtures of anatase and rutile prepared by different mixing methods shown that good contact of ST-21 and ST-G1 particles reduces the reaction efficiency. This suggests that the particle hetero-contact degree may affect the photocatalytic activity.

4.5 References

- Bickley 1991** Bickley R I, Gonzalez-Carreno T, Lees J S, et al. A structural investigation of titanium dioxide photocatalysts[J]. *Journal of Solid state chemistry*, **1991**, 92(1): 178-190.
- Kamat 1993** Kamat P V. Photochemistry on nonreactive and reactive (semiconductor) surfaces[J]. *Chemical Reviews*, **1993**, 93(1): 267-300.
- Hurum 2003** Hurum D C, Agrios A G, Gray K A, et al. Explaining the enhanced photocatalytic activity of Degussa P25 mixed-phase TiO₂ using EPR[J]. *The Journal of Physical Chemistry B*, **2003**, 107(19): 4545-4549.
- Ohno 2003** Ohno T, Tokieda K, Higashida S, et al. Synergism between rutile and anatase TiO₂ particles in photocatalytic oxidation of naphthalene[J]. *Applied Catalysis A: General*, **2003**, 244(2): 383-391.
- Sun 2018** Sun X, Chang Y, Cheng Y, et al. Band alignment-driven oxidative injury to the skin by anatase/rutile mixed-phase titanium dioxide nanoparticles under sunlight exposure[J]. *Toxicological Sciences*, **2018**, 164(1): 300-312.
- Siiriä 2009** Siiriä S, Yliruusi J. Determining a value for mixing: Mixing degree[J]. *Powder Technology*, **2009**, 196(3): 309-317.
- Cleary 1998** Cleary P W, Metcalfe G, Liffman K. How well do discrete element granular flow models capture the essentials of mixing processes?[J]. *Applied Mathematical Modelling*, **1998**, 22(12): 995-1008.
- Suetsugu 1990** Suetsugu Y, Kikutani T, Kyu T, et al. An experimental technique for characterizing dispersion in compounds of particulates in thermoplastics using small-angle light scattering[J]. *Colloid and Polymer Science*, **1990**, 268(2): 118-131.
- Bur 2004** Bur A J, Roth S C, Lee Y H, et al. A dielectric slit die for in-line monitoring of polymer compounding[J]. *Review of scientific instruments*, **2004**, 75(4): 1103-1109.

Amano 2009 Amano F, Yasumoto T, Prieto-Mahaney O O, et al. Photocatalytic activity of octahedral single-crystalline mesoparticles of anatase titanium (IV) oxide[J]. *Chemical communications*, **2009** (17): 2311-2313.

Yeoh 2005 Yeoh S L, Papadakis G, Yianneskis M. Determination of mixing time and degree of homogeneity in stirred vessels with large eddy simulation[J]. *Chemical Engineering Science*, **2005**, 60(8-9): 2293-2302.

Kim 2007 Kim D, Lee J S, Barry C M F, et al. Microscopic measurement of the degree of mixing for nanoparticles in polymer nanocomposites by TEM images[J]. *Microscopy research and technique*, **2007**, 70(6): 539-546.

5.1 Conclusions

Generally, most metal-oxides are categorized as semiconductors according to their electronic energy structure and the band structure, which impact the physical and chemical properties of metal oxides, is very important, though it seems the real band structure of metal oxides is still speculative and only conduction-band bottom (CBB) and valence-band top (VBT) positions have been discussed. The "hetero-contact degree" here indicate quantitative measurement of "heterogeneous contact state" which have been suggested to be decisive factor influencing the performance of materials is a new concept and has not been measured so far. A novel method for identification and characterization of metal-oxide powders with energy-resolved distribution of electron traps (ERDT) measured by reversed double-beam photoacoustic spectroscopy (RDB-PAS) has been developed. In this study, ERDT analysis using RDB-PAS is expected to be applicable to estimation of band structure of metal-oxide samples and provides quantitative measurement of the hetero-contact degree.

In chapter 2, I obtained experimental evidence of interparticle spatial overlapping of orbitals to result in interparticle charge-transfer excitation (ICTE), that is, photoexcitation from the h-DOS(VB) of the higher h-DOS(VB) sample to all ETs at an anatase-rutile interface proved by energy-resolved distribution of electron traps (ERDT) measured by reversed double-beam photoacoustic spectroscopy (RDB-PAS). The detail energy-resolved distribution of electron traps (ERDT) analyses of various anatase-rutile mixtures revealed that all of the photoexcitation occurred from h-DOS in valence band of rutile in thoroughly mixed sample and h-DOS of rutile was located ca. 0.19 eV higher than that of anatase. This is the first experimental results of practical h-DOS, which enable to cause photoabsorption, of materials. In addition, the ICTE analysis suggested a new concept, hetero-contact degree, which could be quantitatively evaluated by comparison of ERDT patterns of mixture sample to simulation patterns with thoroughly adjoined mixture particles and non-contacted particles.

In chapter 3, the ΔE_{\max} values for most mixtures with rutile and anatase prepared by mix-H were 0.18–0.19 eV. Due to the fact that the ΔE_{\max} obtained from the ERDT pattern with homogeneously mixing samples was constant with change in the anatase content, the constant ΔE_{\max} reflects the energy difference between h-DOS (VB)s of anatase and rutile in their mixture samples. Anatase and rutile particles isolated from HomoP25 by

chemical dissolution method were characterized by RDB-PAS to estimate their band structure. The h-DOS(VB) of isolated-rutile (RUT) is the same with most commercial rutile. However, the isolated-anatase (ANA) shows an interesting h-DOS(VB) position that is ca. 0.12 eV higher than most commercial titania. Thus, RDB-PAS analysis of ERDT patterns of mixtures of different titania samples is expected to be a novel method to clarify the relative band position of semiconducting metal oxides such as titania.

In chapter 4, ERDT analysis of various anatase-rutile mixtures provided quantitative measurement of "hetero-contact degree" (how much proportion of one kind of particles (anatase in this study) are electronically contacted with the other kind of particles (rutile in this study)). This is a new concept and has not been measured so far, because such quantitative measurement requires macroscopic analysis collecting the information on particle contact; XRD and BET are representative macroscopic powder analyses, but they give no information on anatase-rutile particle contact, SEM might give some information on anatase-rutile particle contact, but it is microscopic and no average can be obtained.

In conclusion, I obtained experimental evidence of interparticle spatial overlapping of orbitals to result in interparticle charge-transfer excitation (ICTE) at an anatase-rutile interface through ERDT measured by reversed double-beam photoacoustic spectroscopy. The detail ERDT analyses of various anatase-rutile mixtures revealed that all of the photo-excitation occurred from h-DOS in valence band of rutile in thoroughly mixed sample and h-DOS of rutile was located ca. 0.2 eV higher than that of anatase. ERDT analysis using RDB-PAS is expected to be a novel method to clarify the relative band position of semiconducting metal oxides such as titania. In addition, the ERDT analysis suggested a novel concept, hetero-contact degree in this study, could be quantitatively evaluated.

5.2 *Future Aspects*

Since the experimental evidence of interparticle charge-transfer excitation (ICTE) at an anatase-rutile interface was obtained in this study, ERDT analysis using RDB-PAS is expected to be applicable to characterize metal oxide composite materials which are widely used for photocatalysts, solar cells and catalysts. The state of mixing and contact between particles in nanocomposite materials might be evaluated by ERDT analysis. Since the sensitivity to the contact state of different kinds of crystallite, the ERDT analysis is expected to be used to study the conversion process of different crystallite, such as the conversion process of anatase to rutile under high temperature calcination. In this study, I mainly investigated the band structure of titania samples. The band structure of various semiconducting metal oxides should be estimated using this novel analysis technique.

5.3 *Original Papers Covering This Thesis*

Shen, Y., Nitta, A., Takashima, M., & Ohtani, B. Do Particles Interact Electronically?—Proof of Interparticle Charge-Transfer Excitation between Adjoined Anatase and Rutile Particles[J]. *Chemistry Letters*, 2021, 50(1): 80-83.

Acknowledgement

It is an unforgettable experience for me to spend such a long time on preparing, writing and modifying this thesis. Many people give me a lot of help and professional advice during writing and modifying the thesis. Here, I would like to express my sincere gratitude to them.

My deepest gratitude goes first and foremost to Professor Bunsho Ohtani, my supervisor, who has given me constant support and guidance throughout the whole processes. Not only about the guidance of research and writing thesis, but Professor Ohtani's insights of the nature and principles of scientific research have benefited me a lot.

Secondly, I would like to express my heartfelt gratitude to Associate Professor Ewa Kowalska and Assistant Professor Mai Takashima, who have guided and helped me a lot in the past three years. I am also greatly indebted to the professors at the division of environmental materials science: Professor Yuichi Kamiya, Professor Ichizo Yagi, who have instructed and helped me during modifying the thesis.

Thirdly, I want to thank all the members of the Ohtani laboratory who gave me their help in listening to me and helping me work out my problems during the difficult course of this thesis. I also thank the staff of Technical Division in Institute for Catalysis, Hokkaido University for modifying the measurement apparatus of RDB-PAS.

At last, I will give the deepest gratitude to my beloved family and friends for their loving considerations and great confidence in me all through these years.